

Generalized Diffusion Detector: Mining Robust Features from Diffusion Models for Domain-Generalized Detection

Boyong He^{1*}, Yuxiang Ji^{1*}, Qianwen Ye², Zhuoyue Tan¹, Liaoni Wu^{1,2†},

¹*Institute of Artificial Intelligence, Xiamen University*

²*School of Aerospace Engineering, Xiamen University*

{boyonghe, yuxiangji, yeqianwen, tanzhuoyue}@stu.xmu.edu.cn
wuliaoni@xmu.edu.cn[†]

Abstract

Domain generalization (DG) for object detection aims to enhance detectors' performance in unseen scenarios. This task remains challenging due to complex variations in real-world applications. Recently, diffusion models have demonstrated remarkable capabilities in diverse scene generation, which inspires us to explore their potential for improving DG tasks. Instead of generating images, our method extracts multi-step intermediate features during the diffusion process to obtain domain-invariant features for generalized detection. Furthermore, we propose an efficient knowledge transfer framework that enables detectors to inherit the generalization capabilities of diffusion models through feature and object-level alignment, without increasing inference time. We conduct extensive experiments on six challenging DG benchmarks. The results demonstrate that our method achieves substantial improvements of 14.0% mAP over existing DG approaches across different domains and corruption types. Notably, our method even outperforms most domain adaptation methods without accessing any target domain data. Moreover, the diffusion-guided detectors show consistent improvements of 15.9% mAP on average compared to the baseline. Our work aims to present an effective approach for domain-generalized detection and provide potential insights for robust visual recognition in real-world scenarios. The code is available at [Generalized Diffusion Detector](#)

1. Introduction

Object detection stands as a fundamental task in computer vision and has achieved remarkable technological breakthroughs in recent years. Most object detection methods, including CNN [51, 64, 65, 76] and transformer-

based [5, 100] detectors assume consistent distributions between training and testing data. However, in practice, detectors face significant challenges from domain shifts and environmental variations, and the performance often deteriorates substantially when deployed in unseen scenarios [11, 95].

Domain generalization [42, 43, 79] and adaptation [3, 18, 31, 50] methods have been developed to address these challenges. Mainstream approaches include semi-supervised learning with pseudo-labels [3, 6, 18, 50], feature alignment via adversarial training [11, 50, 71, 83], and style transfer techniques [23, 98]. However, these adaptation methods require target domain data during training, limiting their practical applications. This has led to increased interest in domain generalization through data augmentation [16, 29, 41, 94], adversarial training [44, 99], and meta-learning [1, 20]. While recent advances in foundation models like ClipGap [77] have shown promising results, building robust detectors remains challenging.

Inspired by the remarkable capabilities of diffusion models [28, 67, 73] in handling visual variations, we propose to leverage them for domain-generalized detection. We extract and fuse multi-timestep intermediate features during the diffusion process to construct a diffusion-based detector that learns domain-invariant representations. However, directly applying these models introduces significant computational overhead due to the multi-step feature extraction process, limiting their practical deployment.

To address this limitation while preserving their strong generalization advantages, we develop an efficient knowledge transfer framework that enables lightweight detectors to inherit capabilities from diffusion-based detectors. Specifically, our framework consists of feature-level alignment using correlation-based matching and object-level alignment through shared region proposals, allowing conventional detectors to learn both domain-invariant features and robust detection capabilities. Through feature and

*Equal contribution.

†Corresponding author.

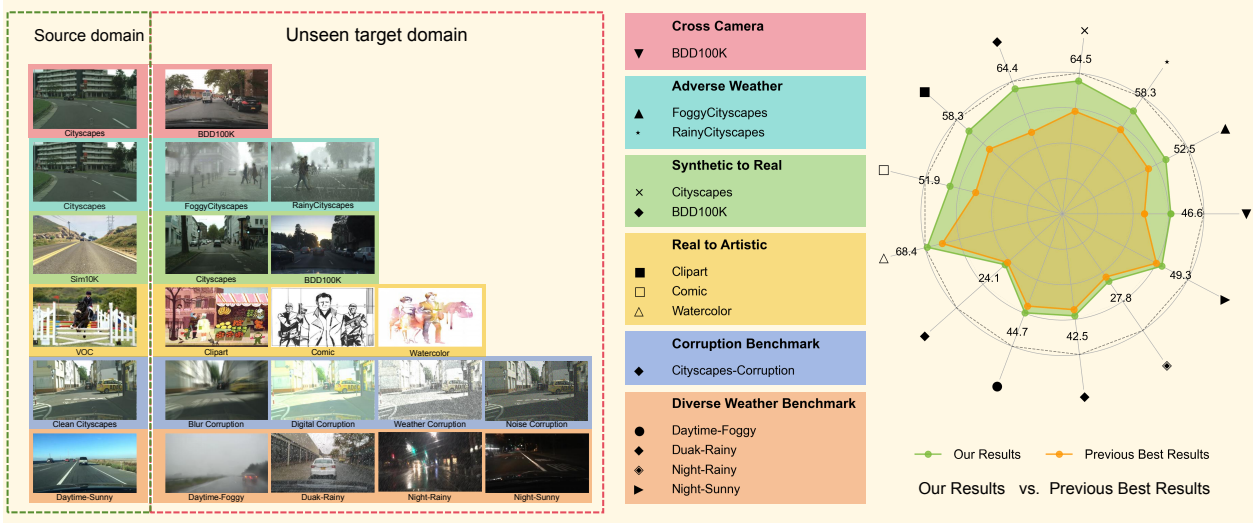


Figure 1. **Left:** Six DG benchmarks used in our paper. The sample images demonstrate substantial domain shifts between source and target distributions. **Right:** Compared with previous SOTA methods, our approach achieves superior performance across all 13 datasets from six benchmarks.

object-level alignment, conventional detectors can achieve improved generalization without increasing inference time. Our work pioneers the application of diffusion models in domain-generalized detection, demonstrating their potential in enhancing detector generalization through knowledge distillation.

We conduct comprehensive experiments on six challenging DG benchmarks as shown in Fig. 1: Cross Camera, Adverse Weather, Synthetic to Real, Real to Artistic, Diverse Weather Benchmark, Corruption Benchmark. Experimental results demonstrate that our diffusion-based detector achieves consistent improvements across these benchmarks, with average performance gains of $\{18.6, 15.0, 27.2, 16.4, 2.3, 4.7\}$ % mAP compared to previous methods, even outperforming most domain adaptation methods that have access to target domain data. Moreover, through our proposed feature-level and object-level learning framework, diffusion-guided detectors obtain significant improvements of $\{20.8, 21.4, 24.6, 9.9, 5.3, 13.8\}$ % mAP compared to their baselines. These results validate the effectiveness of leveraging diffusion models for domain-generalized detection and provide a promising direction for building robust detectors in real-world scenarios.

The main contributions of this work can be summarized as follows:

- This work introduces diffusion models into domain-generalized detection. The inherent denoising mechanism and powerful representation capabilities of diffusion models are utilized to extract domain-invariant features for robust detection.
- To address the computational overhead, we propose a simple yet effective knowledge transfer framework.

This framework enables detectors to inherit strong generalization capabilities through feature-level alignment and object-level learning, maintaining efficient inference time.

- Comprehensive experiments on six DG benchmarks demonstrate significant improvements over previous approaches in various scenarios. The findings provide valuable insights for robust visual recognition tasks.

2. Related Work

2.1. Domain generalization for object detection

Domain adaptation methods for object detection focus on adversarial feature alignment [11, 50, 71, 83] and consistency-based learning with pseudo labels [3, 6, 18, 50]. However, these approaches inherently require target domain data during training. Domain generalization methods have been explored through data augmentation [15, 16, 29, 94], adversarial training [44, 99], and meta-learning [1, 20] to enhance model robustness through style transfer and domain shift simulation. Recent works [16, 41, 53, 82, 96] extend these strategies to domain-generalized detection through multi-view learning, specialized augmentation and causal learning. Additionally, ClipGap [77] demonstrates the potential of foundation models by leveraging CLIP [61]. These advances inspire us to explore diffusion models as foundation models, harnessing their inherent generalization capabilities for domain-generalized detection.

2.2. Diffusion models and applications

Recent studies demonstrate that diffusion models [21, 28, 62, 67, 70, 73] not only excel in image generation but

also exhibit unique advantages in representation learning [2, 24, 84]. The noise-adding and denoising mechanism enables effective handling of visual perturbations like noise, blur, and illumination changes [56, 75]. These properties suggest the potential of diffusion models in addressing domain generalization challenges. Specifically, the intermediate features during diffusion contain rich semantic information [56], while the denoising process naturally builds robustness against various perturbations [75]. Recent works like [2, 24, 36] further demonstrate the effectiveness of diffusion-based representations in various vision tasks. These promising properties motivate us to leverage diffusion models for domain-generalized detection, and further inspire us to explore transferring their superior capabilities to other detectors.

3. Method

3.1. Overview

In this section, we introduce our approach for domain generalization detection. The proposed method leverages a diffusion model as feature extractor to learn domain-robust representations through its iterative process. A two-level alignment mechanism is designed to transfer knowledge from the diffusion model to standard detectors: feature-level alignment for domain-invariant patterns and object-level alignment for accurate detection across domains. The overall framework is illustrated in Fig. 3.

In the following subsections, we first present the problem formulation and introduce the diffusion model basics in Sec. 3.2. The feature extraction and fusion strategy from diffusion models is described in Sec. 3.3. Our two-level alignment approach, including feature-level alignment (Sec. 3.4) and object-level alignment (Sec. 3.5), guides standard detectors to learn robust representations while maintaining accurate detection. The overall training objectives integrating detection losses with alignment constraints are detailed in Sec. 3.6.

3.2. Preliminaries

DG for detection: Let $\mathcal{S} = \{\mathbf{x}_s^i, \mathbf{y}_s^i\}_{i=1}^{N_s}$ denote the source domain with N_s labeled samples, where \mathbf{x}_s^i represents an image and \mathbf{y}_s^i represents the corresponding bounding box annotations. Let $\mathcal{T} = \{\mathbf{x}_t^j\}_{j=1}^{N_t}$ denote the target domain with N_t unlabeled images. The source and target samples are drawn from different distributions $P_{\mathcal{S}}$ and $P_{\mathcal{T}}$, with discrepancies in image distributions (e.g., style, scene), label distributions (e.g., shapes, density), and sample sizes. The goal is to learn robust representations from the labeled source domain that generalize well to the unseen target domain.

Diffusion Model: The diffusion process gradually converts source domain images \mathbf{x}_s^i into pure noise through a fixed

Markov chain of T steps. At each time step $t \in [0, T]$, Gaussian noise is progressively added to obtain the noisy samples \mathbf{x}_t . The forward process is formulated as:

$$\mathbf{x}_t = \sqrt{\bar{\alpha}_t} \mathbf{x}_0 + \sqrt{1 - \bar{\alpha}_t} \epsilon \quad (1)$$

where $\epsilon \sim \mathcal{N}(0, \mathbf{I})$, and $\bar{\alpha}_t$ represents the cumulative product of noise schedule $\{\alpha_t\}_{t=1}^T$ controlling the noise magnitude. During training, a neural network \mathcal{F}_θ learns to estimate the added noise from noisy observations \mathbf{x}_t conditioned on time step t . The network is optimized to minimize the discrepancy between predicted and actual noise. At inference, the model reverses this process by iteratively denoising pure noise through refinement steps until obtaining the final output $\hat{\mathbf{x}}_0$.

3.3. Multi-timestep Feature Extraction and Fusion

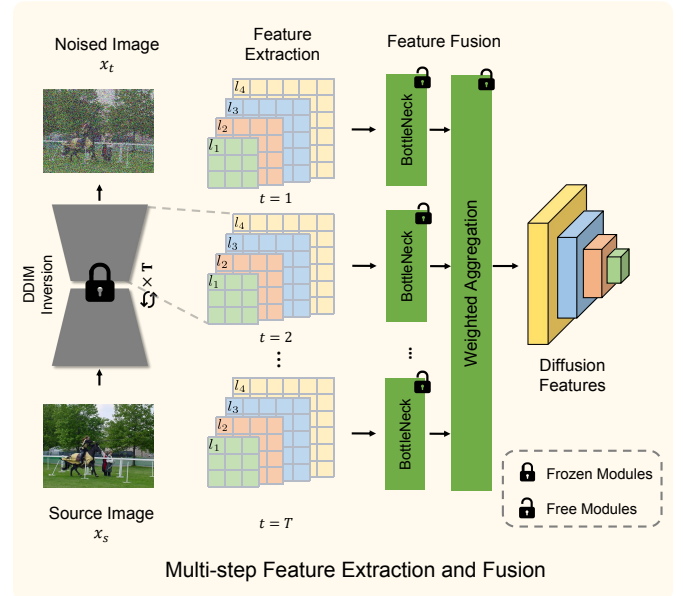


Figure 2. Overview of multi-timestep feature extraction and fusion. Multi-scale features are extracted from a frozen diffusion model at different timesteps, then processed through trainable bottleneck structures and weighted aggregation module to obtain the final hierarchical features.

Feature Extraction via Diffusion: The inherent characteristics of diffusion models' intermediate representations make them particularly suitable for domain-invariant feature learning. During the denoising process, the noise predictor \mathcal{F}_θ accumulates multi-scale semantic information by modeling data variations at different noise levels.

To leverage these properties, we extract and aggregate intermediate features from a sequence of time steps during the forward diffusion process. Specifically, given a source image \mathbf{x}_s^i , we progressively add noise following $\mathbf{x}_s^i \rightarrow \mathbf{x}_1 \rightarrow \dots \rightarrow \mathbf{x}_t$, where $t \in \{1, 2, \dots, T\}$. At

each time step t , we extract features from the four upsample stages of \mathcal{F}_θ , denoted as $\mathbf{s}_t \in \mathbb{R}^{C_{l,k} \times H_{l,k} \times W_{l,k}}$, where for each layer $l \in \{1, 2, 3, 4\}$, we extract three intermediate features ($k = 1, 2, 3$) from the middle of the layer. The feature dimensions are defined as $C_{l,k}$, $H_{l,k}$, and $W_{l,k}$ based on the corresponding layer architecture. This process captures the representation of the transition $\mathbf{x}_{t-1} \rightarrow \mathbf{x}_t$ and generates a multi-timestep feature sequence $\{\mathbf{s}_t\}_{t=1}^T$ for each input image.

Multi-timestep Feature Fusion: For each timestep, features first go through individual bottleneck structures to align dimensions. A weighted aggregation module then combines features across timesteps with learnable weights as shown in Fig. 2. The fused features form a feature pyramid containing four levels with increasing channel dimensions $C_l \in \{C_1, C_2, C_3, C_4\}$ where $C_l = 256 \times 2^{l-1}$, and corresponding spatial resolutions $H_l \times W_l$ where $H_l = H/2^{l+1}$ and $W_l = W/2^{l+1}$ for $l \in \{1, 2, 3, 4\}$, with H and W being the height and width of input image respectively.

3.4. Feature level imitation and alignment

We construct our detector based on the features extracted from the diffusion model as described above. Specifically, we employ Faster R-CNN [65] with all default parameters unchanged and train it exclusively on the source domain to obtain $\mathcal{F}_{\text{diff}}$.

Motivation: Common detectors $\mathcal{F}_{\text{comm}}$ tend to overfit source domain data, limiting their generalization to unseen domains. To address this, we propose leveraging knowledge from diffusion-based detector $\mathcal{F}_{\text{diff}}$ through a two-level alignment approach. Through aligning both feature distributions and object predictions, we expect $\mathcal{F}_{\text{comm}}$ to learn more domain-invariant representations while preserving its detection capability.

Feature alignment: Due to the inherent feature distribution differences between diffusion-based and standard detectors, we adopt PKD [4] for feature alignment, which enables robust cross-architecture knowledge transfer through correlation-based matching.

We extract FPN features $\mathcal{M}_{\text{comm}}^l$ and $\mathcal{M}_{\text{diff}}^l$ from the ResNet [25] of $\mathcal{F}_{\text{comm}}$ and the multi-timestep diffusion feature extraction network in $\mathcal{F}_{\text{diff}}$ respectively. Both features have dimensions $\mathbb{R}^{B \times C \times H_l \times W_l}$ at pyramid level l , where B is the batch size, C is the number of channels, and $H_l \times W_l$ represents the spatial dimensions. With $\hat{\mathcal{M}}$ denoting normalized features, the alignment loss is defined as:

$$\mathcal{L}_{\text{align}} = \sum_{l=1}^L \frac{1}{N_l} \|\hat{\mathcal{M}}_{\text{comm}}^l - \hat{\mathcal{M}}_{\text{diff}}^l\|_2^2 \quad (2)$$

Cross feature adaptation: To address the potential instability of direct feature alignment between heterogeneous models, we propose to feed $\mathcal{M}_{\text{diff}}$ into $\mathcal{F}_{\text{comm}}$'s detection

heads, enabling stable adaptation while preserving the original detection pipeline. The cross feature loss is defined as:

$$\mathcal{L}_{\text{cross}} = \mathcal{L}_{\text{comm}}^{\text{rpn}}(\mathcal{M}_{\text{diff}}; \theta_{\text{comm}}) + \mathcal{L}_{\text{comm}}^{\text{roi}}(\mathcal{M}_{\text{diff}}; \theta_{\text{comm}}) \quad (3)$$

where $\mathcal{L}_{\text{comm}}^{\text{rpn}}$ combines objectness classification and box regression losses for RPN, and $\mathcal{L}_{\text{comm}}^{\text{roi}}$ combines classification and box regression losses for ROI head, following the standard Faster R-CNN detection losses.

3.5. Domain-invariant Object-level Knowledge Transfer

Beyond feature-level alignment, we aim to enhance $\mathcal{F}_{\text{comm}}$'s object detection capability in unseen domains by transferring task-relevant knowledge from $\mathcal{F}_{\text{diff}}$. However, this presents two challenges: (1) target domain data is unavailable during training under the DG setting, and (2) traditional knowledge distillation methods are not directly applicable due to the heterogeneous architectures between $\mathcal{F}_{\text{comm}}$ and $\mathcal{F}_{\text{diff}}$.

Shared ROI Feature Propagation: Inspired by CrossKD [78], we propose to align object-level predictions through shared region proposals. We first generate candidate regions $\mathcal{R}_{\text{roi}} \in \mathbb{R}^{N \times 4}$ using the RPN of $\mathcal{F}_{\text{comm}}$, where N is the number of proposals. These regions are used to pool features from both detectors, yielding fixed-size features $\mathcal{M}_{\text{comm}}^{\text{roi}}$ and $\mathcal{M}_{\text{diff}}^{\text{roi}} \in \mathbb{R}^{N \times d}$, where d is the feature dimension. The spatially aligned features are then fed into diffusion detector's branches:

$$\begin{aligned} \mathbf{P}_{\text{cat}} &= \mathcal{F}_{\text{diff}}^{\text{cls}}(\mathcal{M}_{\text{diff}}^{\text{roi}}), & \mathbf{P}_{\text{bbox}} &= \mathcal{F}_{\text{diff}}^{\text{reg}}(\mathcal{M}_{\text{diff}}^{\text{roi}}) \\ \mathbf{Q}_{\text{cat}} &= \mathcal{F}_{\text{diff}}^{\text{cls}}(\mathcal{M}_{\text{comm}}^{\text{roi}}), & \mathbf{Q}_{\text{bbox}} &= \mathcal{F}_{\text{diff}}^{\text{reg}}(\mathcal{M}_{\text{comm}}^{\text{roi}}) \end{aligned} \quad (4)$$

where $\mathbf{P}_{\text{cat}}, \mathbf{Q}_{\text{cat}} \in \mathbb{R}^{N \times (C+1)}$ denote the class logits for C object categories plus background, and $\mathbf{P}_{\text{bbox}}, \mathbf{Q}_{\text{bbox}} \in \mathbb{R}^{N \times 4}$ represent the predicted box coordinates.

Classification Knowledge Transfer: For classification knowledge transfer, we use KL divergence with temperature scaling:

$$\mathcal{L}_{\text{cls}} = \frac{1}{N} \sum_{i=1}^N \tau^2 D_{KL}(\mathbf{Q}_{\text{cat}}^i \parallel \mathbf{P}_{\text{cat}}^i) \quad (5)$$

where $\mathbf{Q}_{\text{cat}}^i, \mathbf{P}_{\text{cat}}^i$ are temperature-scaled softmax outputs for the i -th proposal, and τ is the temperature parameter.

Regression Knowledge Transfer: For box regression, we use L1 loss:

$$\mathcal{L}_{\text{reg}} = \frac{1}{N} \sum_{i=1}^N \|\mathbf{Q}_{\text{bbox}}^i - \mathbf{P}_{\text{bbox}}^i\|_1 \quad (6)$$

Through this object-level knowledge transfer mechanism, $\mathcal{F}_{\text{comm}}$ learns domain-invariant detection capabilities

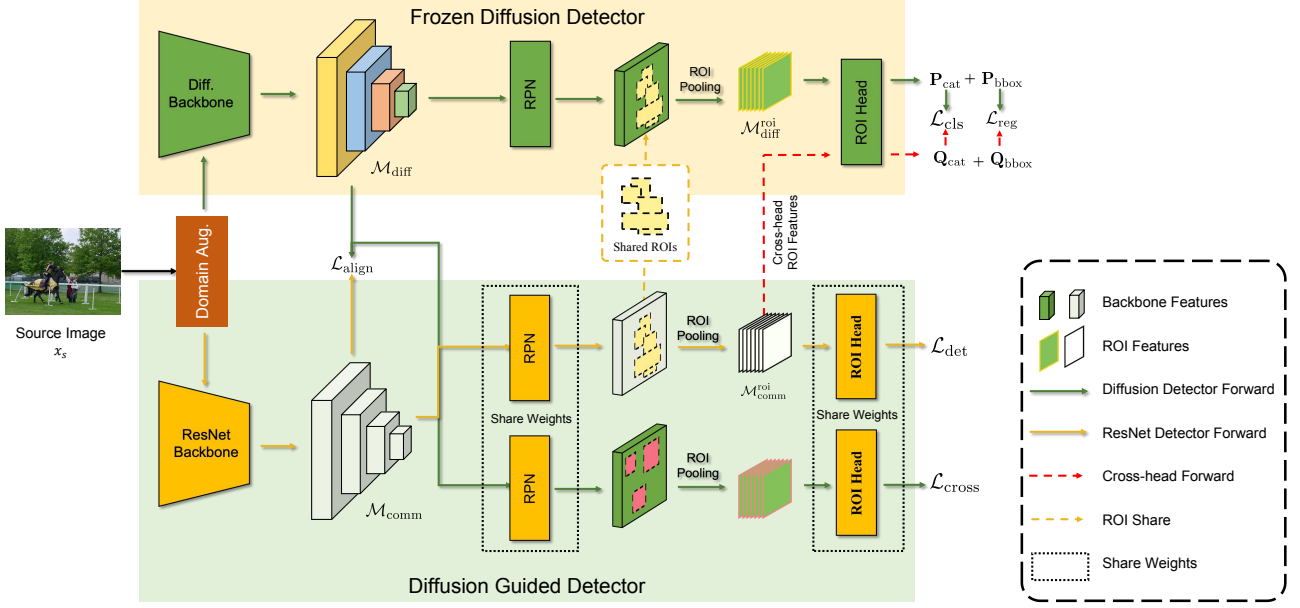


Figure 3. Overview of the proposed methods. The framework consists of a frozen diffusion detector (**top**) and a trainable ResNet-based detector (**bottom**). Knowledge transfer is achieved through feature-level alignment ($\mathcal{L}_{\text{align}}$, $\mathcal{L}_{\text{cross}}$) and object-level prediction alignment using shared ROIs (\mathcal{L}_{cls} and \mathcal{L}_{reg}).

from $\mathcal{F}_{\text{diff}}$ via ROI-level alignment. By sharing the same detection head while processing features from different sources, we encourage $\mathcal{F}_{\text{comm}}$ to extract domain-agnostic object features that can generalize well across domains.

3.6. Joint Optimization Objective

The overall objective combines supervised detection learning with feature-level and object-level alignments:

$$\mathcal{L}_{\text{total}} = \underbrace{\mathcal{L}_{\text{det}}(\mathcal{F}_{\text{comm}}(\mathbf{x}_s), \mathbf{y}_s)}_{\text{supervised learning on source domain}} + \lambda_{\text{feature}} \underbrace{(\mathcal{L}_{\text{align}} + \mathcal{L}_{\text{cross}})}_{\text{feature-level alignment}} + \lambda_{\text{object}} \underbrace{(\mathcal{L}_{\text{cls}} + \mathcal{L}_{\text{reg}})}_{\text{object-level alignment}} \quad (7)$$

where \mathcal{L}_{det} is the detection loss on source domain data $(\mathbf{x}_s, \mathbf{y}_s)$, with λ_{feature} and λ_{object} being the weights for feature-level and object-level alignment respectively.

4. Experiments

4.1. DG Detection Benchmarks

Cross Camera. Train on Cityscapes [14] (2,975 training images from 50 cities) and test on BDD100K [89] day-clear split with 7 shared categories following SWDA [71], evaluating generalization across diverse urban scenes.

Adverse Weather. Train on Cityscapes [14] and test on FoggyCityscapes [72] and RainyCityscapes [32] (synthesized by adding fog and rain effects), using the challenging

0.02 split setting for FoggyCityscapes to evaluate robustness under degraded visibility conditions.

Synthetic to Real. Train on Sim10K [38] (10K synthetic driving scenes rendered by GTA-V) and test on Cityscapes [14] and BDD100K [89] for the *car* category, examining synthetic-to-real transfer capability.

Real to Artistic. Train on VOC [22] (16,551 real-world images from 2007 and 2012) and test on Clipart [35] (1K images, 20 categories), Comic [35] (2K images, 6 categories), and Watercolor [35] (2K images, 6 categories) following [50].

Diverse Weather benchmark. Train on Daytime-Sunny (26,518 images) and test on four challenging conditions: Night-Sunny (26,158 images), Night-Rainy (2,494 images), Dusk-Rainy (3,501 images), and Daytime-Foggy (3,775 images) following [80], evaluating robustness across diverse weather and lighting scenarios. We follow settings from OADG [41] for comparison.

Corruption benchmark. A comprehensive test-only benchmark [58] with 15 different corruption types at 5 severity levels for Cityscapes [14], spanning noise, blur, weather, and digital perturbations to evaluate model robustness systematically. We follow settings from OADG [41] for comparison.

4.2. Implementation Details

Training settings: We adopt Faster R-CNN [65] with ResNet101 [25] backbone pretrained on ImageNet [69] as

Table 1. Cross Camera DG and DA Results (%) on BDD100K.

Methods	Bike	Bus	Car	Motor	Psn.	Rider	Truck	mAP
DG methods (without target data)								
CDSR [80] (CVPR'22)	22.9	20.5	33.8	14.7	18.5	23.6	18.2	21.7
SHADE [92] (ECCV'22)	25.1	19.0	36.8	18.4	24.1	24.9	19.8	24.0
SRCD [63] (TNNLS'24)	24.8	21.5	38.7	19.0	25.7	28.4	23.1	25.9
MAD [85] (CVPR'23)	-	-	-	-	-	-	-	28.0
DA methods (with unlabeled target data)								
TDD [27] (CVPR'22)	28.8	25.5	53.9	24.5	39.6	38.9	24.1	33.6
PT [10] (ICML'22)	28.8	33.8	52.7	23.0	40.5	39.9	25.8	34.9
SIGMA [48] (CVPR'22)	26.3	23.6	64.1	17.9	46.9	29.6	20.2	32.7
SIGMA++ [49] (TPAMI'23)	27.1	26.3	65.6	17.8	47.5	30.4	21.1	33.7
NSA [97] (ICCV'23)	-	-	-	-	-	-	-	35.5
HT [18] (CVPR'23)	38.0	30.6	63.5	28.2	53.4	40.4	27.4	40.2
Ours (DG settings)								
Diff. Detector (SD-1.5)	38.9	31.0	71.5	37.6	61.5	47.0	38.5	46.6
Diff. Detector (SD-2.1)	38.0	<u>33.6</u>	69.9	36.6	62.1	46.3	34.2	45.8
Diff. Guided (SD-1.5)	38.4	33.4	72.0	38.3	60.3	47.0	35.0	46.3+20.9
Diff. Guided (SD-2.1)	38.5	32.6	71.8	37.5	60.2	46.7	35.3	46.1+20.7

baseline detector. Models are trained for 20K iterations with batch size 16, learning rate 0.02 and SGD optimizer. We use EMA updated model for stable training. Other settings follow MMDetection defaults [9].

Evaluation metrics: We report AP₅₀ for individual categories and mAP across categories. For Corruption benchmark [58], we additionally report mPC (average AP_{50:95} across 15 corruptions with 5 levels) and rPC (ratio between mPC and clean performance).

Domain augmentation: Following [24, 50], we employ *Strong Augmentation* including both color transformations (color jittering, contrast, equalization, sharpness) and spatial transformations (rotation, shear, translation). Additionally, we design domain-level augmentation strategies by applying *FDA* [87], *Histogram Matching*, and *Pixel Distribution Matching* between source domain images to generate diverse training samples.

Hyper-parameters: We set diffusion steps $T = 5$ and max-timestep as 500 for artistic benchmarks and 100 for other benchmarks as described in Sec. 3.3. The loss weights are set as $\lambda_{\text{feature}} = 0.5$ and $\lambda_{\text{object}} = 1$ in Eq. 7.

4.3. Results and Comparisons

We compare our approach against existing DG methods (target domain unseen) and DA methods (target domain unlabeled). Our results include **Diff. Detector** trained solely on source domain (Sec. 3.3), **SD-1.5** and **SD-2.1** using different StableDiffusion [66] versions, and **Diff. Guided** which applies our alignment approach to Faster R-CNN [65] baseline through **Diff. Detector** as described in Sec. 3.4 and 3.5.

In all tables, **bold** and underline denote the best and second-best results. Yellow background highlights the best average performance. And **+x** indicates mAP(%) gains over baseline.

We conduct extensive experiments across six challenging benchmarks to evaluate our method in Tab. 1, 2, 3,

Table 2. Adverse Weather DG and DA Results (%) on FoggyCityscapes.

Methods	Bus	Bike	Car	Motor	Psn.	Rider	Train	Truck	mAP
DG methods									
FACT [86] (CVPR'21)									
FSDR [33] (CVPR'22)									
MAD [85] (CVPR'23)									
DA methods									
MGA [96] (CVPR'22)									
MTTrans [90] (CVPR'22)									
OADA [88] (CVPR'22)									
MIC [30] (CVPR'23)									
SIGMA++ [49] (TPAMI'23)									
CIGAR [52] (CVPR'23)									
CMT [3] (CVPR'23)									
HT [18] (CVPR'23)									
Ours (DG settings)									
Diff. Detector (SD-1.5)	38.9	31.0	71.5	37.6	61.5	47.0	38.5	46.6	
Diff. Detector (SD-2.1)	38.0	<u>33.6</u>	69.9	36.6	62.1	46.3	34.2	45.8	
Diff. Guided (SD-1.5)	38.4	33.4	72.0	38.3	60.3	47.0	35.0	46.3+20.9	
Diff. Guided (SD-2.1)	38.5	32.6	71.8	37.5	60.2	46.7	35.3	46.1+20.7	
Ours (DG settings)									
Diff. Detector (SD-1.5)		58.2							
Diff. Detector (SD-2.1)		56.1							
Diff. Guided (SD-1.5)		57.9+21.5							
Diff. Guided (SD-2.1)		58.3+21.9							
DA methods									
SWDA [71] (CVPR'19)									
MTTrans [90] (CVPR'22)									
SIGMA [48] (CVPR'22)									
TDD [27] (CVPR'23)									
CMT [3] (CVPR'23)									
SIGMA++ [49] (TPAMI'23)									
CIGAR [52] (CVPR'23)									
NSA [97] (ICCV'23)									
Ours (DG settings)									
Diff. Detector (SD-1.5)		62.8							
Diff. Detector (SD-2.1)		64.5							
Diff. Guided (SD-1.5)		59.7+22.3							
Diff. Guided (SD-2.1)		57.3+19.9							
DA methods									
CDSD [80] (CVPR'22)									
SHADE [92] (CVPR'22)									
SRCD [63] (TNNLS'24)									
Ours (DG settings)									
Diff. Detector (SD-1.5)		58.2							
Diff. Detector (SD-2.1)		56.1							
Diff. Guided (SD-1.5)		57.9+21.5							
Diff. Guided (SD-2.1)		58.3+21.9							
Cityscapes BDD100K									
DG methods									
FACT [86] (CVPR'21)									
FSDR [33] (CVPR'22)									
MAD [85] (CVPR'23)									
DA methods									
SWDA [71] (CVPR'19)									
MTTrans [90] (CVPR'22)									
SIGMA [48] (CVPR'22)									
TDD [27] (CVPR'23)									
CMT [3] (CVPR'23)									
SIGMA++ [49] (TPAMI'23)									
CIGAR [52] (CVPR'23)									
NSA [97] (ICCV'23)									
Ours (DG settings)									
Diff. Detector (SD-1.5)		62.8							
Diff. Detector (SD-2.1)		64.5							
Diff. Guided (SD-1.5)		59.7+22.3							
Diff. Guided (SD-2.1)		57.3+19.9							

Table 3. Adverse Weather DG and DA Results (%) on RainyCityscapes.

Methods	DF	DR	NR	NS	Average
CDSD [80] (CVPR'22)	33.5	28.2	16.6	36.6	28.7
SHADE [92] (CVPR'22)	33.4	29.5	16.8	33.9	28.4
CLIPGap [77] (CVPR'23)	32.0	26.0	12.4	34.4	26.2
SRCD [63] (TNNLS'24)	35.9	28.8	17.0	36.7	29.6
G-NAS [82] (AAA'24)	36.4	35.1	17.4	45.0	33.5
OA-DG [41] (AAA'24)	38.3	33.9	16.8	38.0	31.8
DivAlign [16] (CVPR'24)	37.2	38.1	<u>24.1</u>	42.5	35.5
UFR [53] (CVPR'24)	39.6	33.2	19.2	40.8	33.2
Diff. Detector (SD-1.5)	43.3	42.5	27.8	47.0	40.2
Diff. Detector (SD-2.1)	44.6	41.6	23.2	46.4	39.0
Diff. Guided (SD-1.5)	44.7	37.4	21.7	48.7	38.1+13.9
Diff. Guided (SD-2.1)	44.7	37.1	20.0	49.3	37.8+13.6

4, 6, 5 and 7. Our comprehensive evaluations demonstrate that the diffusion detector consistently achieves SOTA

Table 6. Real to Artistic DG and DA Results (%) on Clipart, Comic, Watercolor.

Methods	Clipart	Comic	Watercolor
<i>DG methods</i>			
Div. (CVPR'24)	33.7	25.5	52.5
DivAlign (CVPR'24)	38.9	33.2	57.4
<i>DA methods</i>			
SWDA (CVPR'19)	–	29.4	53.3
MCRA (ECCV'20)	–	33.5	56.0
I3Net (CVPR'21)	–	30.1	51.5
DBG (ICCV'21)	–	29.7	53.8
AT (CVPR'22)	49.3	–	59.9
D-ADAPT (ICLR'22)	49.0	40.5	–
TIA (CVPR'22)	46.3	–	–
LODS (CVPR'22)	45.2	–	58.2
CIGAR (CVPR'23)	46.2	–	–
CMT (CVPR'23)	47.0	–	–
<i>Ours (DG settings)</i>			
Diff. Detector (SD-1.5)	58.3	51.9	68.4
Diff. Detector (SD-2.1)	51.7	46.6	62.1
Diff. Guided (SD-1.5)	40.8+13.6	29.7+11.6	54.2+12.7
Diff. Guided (SD-2.1)	32.7+5.5	24.9+6.8	50.6+9.1

performance in DG settings and even surpasses most domain adaptation methods that require target domain data. Through effective feature and object alignment, our diffusion guidance mechanism successfully enhances detector generalization under moderate domain gaps. However, its improvement becomes more limited when facing extreme domain shifts, particularly in Real-to-Artistic benchmarks (in Tab. 6).

5. Ablation Studies

Table 10. Model calibration performance with D-ECE [40] metric.

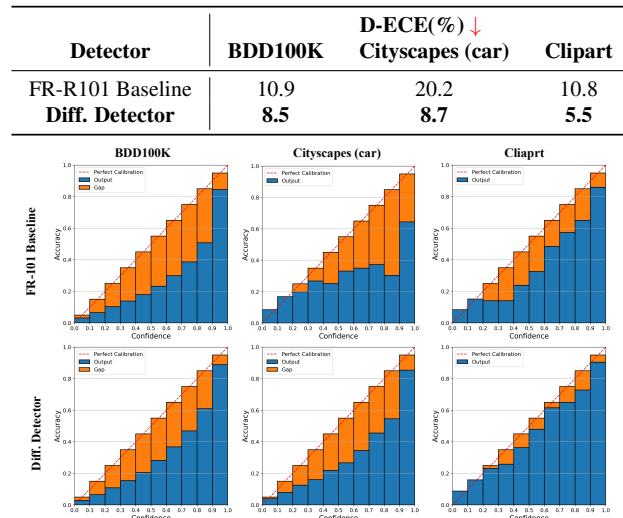


Figure 5. Reliability Diagram on different target domains. Curves closer to the diagonal indicate better performance.

5.1. Studies on Diffusion Detector

Comparison with stronger backbones: We evaluate against recent advanced models [19, 26, 45, 54, 55] under same settings. Results in Tab. 9 demonstrate our diffusion backbone’s superior generalization through effective domain-invariant feature extraction.

We investigate two key parameters for extracting features from diffusion models: the number of diffusion steps T and max timesteps (Sec. 3.3).

Analysis of diffusion steps T : Tab. 8 shows that larger T values improve performance but increase inference time. We set $T = 5$ as default for balancing accuracy and efficiency.

Analysis of max timesteps: Fig. 4 demonstrates that larger timesteps (e.g., 500) benefit benchmarks with severe domain shifts like Real-to-Artistic, while others perform well at timestep 100.

Insights on generalization: Our empirical results reveal two key findings: (1) Without noise diffusion (max timestep 0), the model inherits strong transfer capability from large-scale pre-training, similar to GLIP [45]; (2) The noise-adding and denoising process enhances generalization, with higher noise levels particularly benefiting larger domain shifts through learning domain-invariant features.

5.2. Studies on Diffusion Guided Detector

Analysis of proposed modules: Tab. 11 validates our components’ effectiveness for domain generalization. Domain augmentation yields limited gains (2.7%) for the diffusion detector but significant improvement (11.0%) for baseline, indicating diffusion detector relies more on inherent generalization while trainable-backbone detectors benefit more from diverse training samples.

Feature-level and object-level alignment improve performance by 3.5% and 6.4% respectively, showing effective representation learning under diffusion guidance. The consistent gains (6.1%) with data augmentation further demonstrate our alignment approach’s compatibility with conventional techniques.

Analysis of λ_{feature} and λ_{object} : As shown in Fig. 6, we investigate the impact of different weighting factors λ_{feature} and λ_{object} . We observe that larger weights lead to improved performance on the target domain while slightly degrading the source domain performance. This trade-off suggests an inherent conflict between the model’s ability to fit training data and generalize to unseen target domain data.

5.3. Model Calibration Performance for DG

Our diffusion detector demonstrates superior confidence calibration compared to FR-R101 baseline (Fig. 5, Tab. 10). The Diff. Detector reduces D-ECE [40] to 8.5%, 8.7%, and 5.5% on BDD100K, Cityscapes, and Clipart datasets respectively. As shown in Fig. 5, our calibration curves more

Table 7. Generalization detection Results (%) on Cityscapes Corruption benchmark. (mPC and rPC are defined in Sec. 4.2).

Methods	Noise				Blur			Weather			Digital				mPC \uparrow	rPC \uparrow		
	Clean	Gauss.	Shot	Impulse	Defocus	Glass	Motion	Zoom	Snow	Frost	Fog	Bright	Contrast	Elastic	JPEG	Pixel		
FSCE [74] (CVPR'21)	43.1	7.4	10.2	8.2	23.3	20.3	21.5	4.8	5.6	23.6	37.1	38.0	31.9	40.0	20.4	23.2	21.0	48.7
OA-Mix [41] (AAAI'24)	42.7	7.2	9.6	7.7	22.8	18.8	21.9	5.4	5.2	23.6	37.3	38.7	31.9	40.2	20.2	22.2	20.8	48.7
OA-DG [41] (AAAI'24)	43.4	8.2	10.6	8.4	24.6	20.5	22.3	4.8	6.1	25.0	38.4	39.7	32.8	40.2	22.0	23.8	21.8	50.2
Diff. Detector (SD-1.5)	34.7	20.3	23.2	17.2	26.8	21.7	23.7	3.4	16.6	24.2	32.5	34.4	30.6	33.7	29.1	24.4	24.1	69.5
Diff. Detector (SD-2.1)	34.7	18.4	20.9	15.7	26.2	20.5	21.9	4.0	14.3	22.6	31.4	33.8	29.3	32.5	27.9	21.5	22.7	65.5
Diff. Guided (SD-1.5)	42.1	11.0	13.6	10.8	25.0	14.2	21.4	3.4	5.4	24.0	39.6	40.3	36.3	39.2	18.9	16.0	21.3+5.7	50.5+12.3
Diff. Guided (SD-2.1)	42.2	8.2	10.5	8.2	21.6	12.4	20.1	3.0	3.1	24.5	39.2	39.5	35.8	38.7	23.1	19.6	20.5+4.9	48.6+10.4

Table 8. Testing results and inference costs of different diffusion steps T .

T	BDD	Cityscapes	Clipart	Inference Time (ms)
	100K	(car)	Clipart	
1	28.6	49.8	37.4	270
2	34.9	54.1	48.6	404
5	46.6	62.8	58.3	789
10	47.1	62.6	58.9	1,424
20	45.6	61.4	57.7	2,820

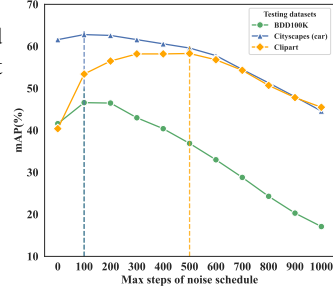


Figure 4. Testing results of different max timesteps.

Table 9. Comparison of Diffusion backbone and stronger models

Models	Clipart	Comic	Watercolor	DF	DR	NR	NS
ConvNeXt-base [55]	43.6	26.6	55.1	39.7	39.2	23.4	45.9
VIT-base [19]	29.5	15.5	43.0	24.8	25.8	11.4	23.0
Swin-base [54]	30.2	18.0	42.6	37.2	38.9	22.6	42.2
MAE (VIT-base) [26]	28.1	16.7	44.4	32.5	32.6	17.0	34.3
Glip (Swin-tiny) [45]	39.2	18.7	50.4	38.5	36.3	20.3	45.5
Diffusion backbone	58.3	51.9	68.4	43.4	42.5	27.8	47.0

Table 11. Ablation studies of our framework components. **Settings**: domain augmentation (**Aug.**), feature-level alignment (**Fea.**), and object-level alignment (**Obj.**). Foggy Cityscapes (**F-C**), Rainy Cityscapes (**R-C**)

Settings	Aug.	Fea.	Obj.	BDD	F-C	R-C	DF	DR	NR	NS
Diff. Detector	✓			44.5	48.0	54.4	41.3	40.4	24.3	43.7
				46.6+2.1	50.1+2.1	58.2+3.8	43.3+2.0	42.5+2.1	27.8+3.5	47.0+3.3
FR-R101				25.4	30.7	36.4	28.8	24.1	12.4	31.4
baseline	✓			36.2+10.8	47.9+17.2	50.1+13.7	39.9+11.1	34.8+10.7	16.4+4.0	41.2+9.8
		✓		29.8+4.4	34.2+3.5	41.2+4.8	34.2+5.4	24.9+0.8	14.4+2.0	35.2+3.8
Diff. Guided		✓		34.9+9.5	38.3+7.6	43.1+6.7	37.2+8.4	26.3+2.2	16.4+4.0	38.1+6.7
	✓	✓		38.1+12.7	40.4+9.7	45.9+9.5	38.6+9.8	28.4+4.3	16.8+4.4	39.5+8.1
	✓	✓	✓	46.3+20.9	52.5+21.8	57.9+21.5	44.7+15.9	37.4+13.3	21.7+9.3	48.7+17.3

closely follow the diagonal line, indicating better alignment between predicted confidence scores and empirical accuracies across domains.

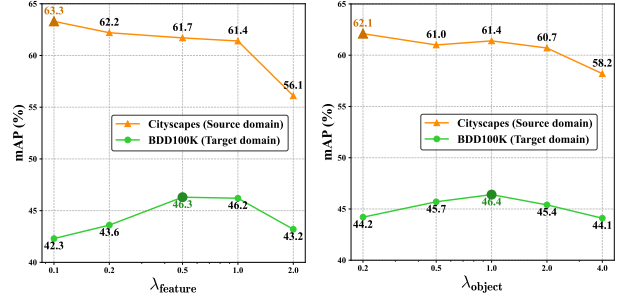


Figure 6. Testing results of λ_{feature} and λ_{object} on source domain and target domain.

5.4. Limitations

Despite achieving strong results across various benchmarks, our diffusion detector faces efficiency challenges. The large parameter count and multi-step denoising process incur substantial computational costs (Tab. 8), limiting its applicability to larger-scale scenarios.

Moreover, while leveraging diffusion models' generalization capability, performance gains remain limited under severe domain shifts (Tab. 6). Future work could explore more efficient architectures and effective learning strategies to better handle extreme domain gaps.

6. Conclusion

This paper addresses DG detection through two key contributions. First, we propose a diffusion detector that extracts domain-invariant representations by fusing multi-step features during diffusion. Second, to enable other detectors to benefit from such generalization capability, we develop a diffusion-guided detector framework that transfers knowledge to conventional detectors through feature and object level alignment. Extensive evaluations on six domain generalization benchmarks demonstrate substantial improvements across different domains and corruption types. Our work not only provides an effective solution for domain-generalized detection but also opens up new possibilities for leveraging diffusion models to enhance visual recognition robustness.

References

- [1] Yogesh Balaji, Swami Sankaranarayanan, and Rama Chellappa. Metareg: Towards domain generalization using meta-regularization. *Advances in neural information processing systems*, 31, 2018. [1](#), [2](#)
- [2] Dmitry Baranchuk, Andrey Voynov, Ivan Rubachev, Valentin Khrulkov, and Artem Babenko. Label-efficient semantic segmentation with diffusion models. In *International Conference on Learning Representations*, 2022. [3](#)
- [3] Shengcao Cao, Dhiraj Joshi, Liang-Yan Gui, and Yu-Xiong Wang. Contrastive mean teacher for domain adaptive object detectors. In *Proceedings of the IEEE/CVF Conference on Computer Vision and Pattern Recognition*, pages 23839–23848, 2023. [1](#), [2](#), [6](#), [3](#)
- [4] Weihao Cao, Yifan Zhang, Jianfei Gao, Anda Cheng, Ke Cheng, and Jian Cheng. Pkd: General distillation framework for object detectors via pearson correlation coefficient. *Advances in Neural Information Processing Systems*, 35:15394–15406, 2022. [4](#), [1](#)
- [5] Nicolas Carion, Francisco Massa, Gabriel Synnaeve, Nicolas Usunier, Alexander Kirillov, and Sergey Zagoruyko. End-to-end object detection with transformers. In *European conference on computer vision*, pages 213–229. Springer, 2020. [1](#)
- [6] Chaoqi Chen, Zebiao Zheng, Xinghao Ding, Yue Huang, and Qi Dou. Harmonizing transferability and discriminability for adapting object detectors. In *Proceedings of the IEEE/CVF conference on computer vision and pattern recognition*, pages 8869–8878, 2020. [1](#), [2](#)
- [7] Chaoqi Chen, Jiongcheng Li, Zebiao Zheng, Yue Huang, Xinghao Ding, and Yizhou Yu. Dual bipartite graph learning: A general approach for domain adaptive object detection. In *Proceedings of the IEEE/CVF International Conference on Computer Vision*, pages 2703–2712, 2021. [2](#)
- [8] Chaoqi Chen, Zebiao Zheng, Yue Huang, Xinghao Ding, and Yizhou Yu. I3net: Implicit instance-invariant network for adapting one-stage object detectors. In *Proceedings of the IEEE/CVF conference on computer vision and pattern recognition*, pages 12576–12585, 2021. [2](#)
- [9] Kai Chen, Jiaqi Wang, Jiangmiao Pang, Yuhang Cao, Yu Xiong, Xiaoxiao Li, Shuyang Sun, Wansen Feng, Ziwei Liu, Jiarui Xu, et al. Mmdetection: Open mmlab detection toolbox and benchmark. *arXiv preprint arXiv:1906.07155*, 2019. [6](#)
- [10] Meilin Chen, Weijie Chen, Shicai Yang, Jie Song, Xinchao Wang, Lei Zhang, Yunfeng Yan, Donglian Qi, Yueteng Zhuang, Di Xie, et al. Learning domain adaptive object detection with probabilistic teacher. In *International Conference on Machine Learning*, pages 3040–3055. PMLR, 2022. [6](#)
- [11] Yuhua Chen, Wen Li, Christos Sakaridis, Dengxin Dai, and Luc Van Gool. Domain adaptive faster r-cnn for object detection in the wild. In *Proceedings of the IEEE conference on computer vision and pattern recognition*, pages 3339–3348, 2018. [1](#), [2](#)
- [12] Yuhua Chen, Haoran Wang, Wen Li, Christos Sakaridis, Dengxin Dai, and Luc Van Gool. Scale-aware domain adaptive faster r-cnn. *International Journal of Computer Vision*, 129(7):2223–2243, 2021. [2](#)
- [13] Sungha Choi, Sanghun Jung, Huiwon Yun, Joanne T Kim, Seungryong Kim, and Jaegul Choo. Robustnet: Improving domain generalization in urban-scene segmentation via instance selective whitening. In *Proceedings of the IEEE/CVF conference on computer vision and pattern recognition*, pages 11580–11590, 2021. [3](#)
- [14] Marius Cordts, Mohamed Omran, Sebastian Ramos, Timo Rehfeld, Markus Enzweiler, Rodrigo Benenson, Uwe Franke, Stefan Roth, and Bernt Schiele. The cityscapes dataset for semantic urban scene understanding. In *Proceedings of the IEEE conference on computer vision and pattern recognition*, pages 3213–3223, 2016. [5](#)
- [15] Ekin D Cubuk, Barret Zoph, Jonathon Shlens, and Quoc V Le. Randaugment: Practical automated data augmentation with a reduced search space. In *Proceedings of the IEEE/CVF conference on computer vision and pattern recognition workshops*, pages 702–703, 2020. [2](#)
- [16] Muhammad Sohail Danish, Muhammad Haris Khan, Muhammad Akhtar Munir, M Saqib Sarfraz, and Mohsen Ali. Improving single domain-generalized object detection: A focus on diversification and alignment. In *Proceedings of the IEEE/CVF Conference on Computer Vision and Pattern Recognition*, pages 17732–17742, 2024. [1](#), [2](#), [6](#), [3](#)
- [17] Jinhong Deng, Wen Li, Yuhua Chen, and Lixin Duan. Unbiased mean teacher for cross-domain object detection. In *Proceedings of the IEEE/CVF Conference on Computer Vision and Pattern Recognition*, pages 4091–4101, 2021. [2](#)
- [18] Jinhong Deng, Dongli Xu, Wen Li, and Lixin Duan. Harmonious teacher for cross-domain object detection. In *Proceedings of the IEEE/CVF Conference on Computer Vision and Pattern Recognition*, pages 23829–23838, 2023. [1](#), [2](#), [6](#)
- [19] Alexey Dosovitskiy, Lucas Beyer, Alexander Kolesnikov, Dirk Weissenborn, Xiaohua Zhai, Thomas Unterthiner, Mostafa Dehghani, Matthias Minderer, Georg Heigold, Sylvain Gelly, et al. An image is worth 16x16 words: Transformers for image recognition at scale. *arXiv preprint arXiv:2010.11929*, 2020. [7](#), [8](#)
- [20] Yingjun Du, Jun Xu, Huan Xiong, Qiang Qiu, Xiantong Zhen, Cees GM Snoek, and Ling Shao. Learning to learn with variational information bottleneck for domain generalization. In *Computer Vision–ECCV 2020: 16th European Conference, Glasgow, UK, August 23–28, 2020, Proceedings, Part X 16*, pages 200–216. Springer, 2020. [1](#), [2](#)
- [21] Patrick Esser, Sumith Kulal, Andreas Blattmann, Rahim Entezari, Jonas Müller, Harry Saini, Yam Levi, Dominik Lorenz, Axel Sauer, Frederic Boesel, et al. Scaling rectified flow transformers for high-resolution image synthesis. In *Forty-first International Conference on Machine Learning*, 2024. [2](#), [4](#)
- [22] Mark Everingham, Luc Van Gool, Christopher KI Williams, John Winn, and Andrew Zisserman. The pascal visual object classes (voc) challenge. *International journal of computer vision*, 88:303–338, 2010. [5](#)
- [23] Ian Goodfellow, Jean Pouget-Abadie, Mehdi Mirza, Bing Xu, David Warde-Farley, Sherjil Ozair, Aaron Courville,

and Yoshua Bengio. Generative adversarial networks. *Communications of the ACM*, 63(11):139–144, 2020. 1

[24] Boyong He, Yuxiang Ji, Zhuoyue Tan, and Liaoni Wu. Diffusion domain teacher: Diffusion guided domain adaptive object detector. In *ACM Multimedia 2024*, 2024. 3, 6, 1

[25] Kaiming He, Xiangyu Zhang, Shaoqing Ren, and Jian Sun. Deep residual learning for image recognition. In *Proceedings of the IEEE conference on computer vision and pattern recognition*, pages 770–778, 2016. 4, 5

[26] Kaiming He, Xinlei Chen, Saining Xie, Yanghao Li, Piotr Dollár, and Ross Girshick. Masked autoencoders are scalable vision learners. In *Proceedings of the IEEE/CVF conference on computer vision and pattern recognition*, pages 16000–16009, 2022. 7, 8

[27] Mengzhe He, Yali Wang, Jiaxi Wu, Yiru Wang, Hanqing Li, Bo Li, Weihao Gan, Wei Wu, and Yu Qiao. Cross domain object detection by target-perceived dual branch distillation. In *Proceedings of the IEEE/CVF Conference on Computer Vision and Pattern Recognition*, pages 9570–9580, 2022. 6

[28] Jonathan Ho, Ajay Jain, and Pieter Abbeel. Denoising diffusion probabilistic models. *Advances in neural information processing systems*, 33:6840–6851, 2020. 1, 2

[29] Minui Hong, Jinwoo Choi, and Gunhee Kim. Stylemix: Separating content and style for enhanced data augmentation. In *Proceedings of the IEEE/CVF conference on computer vision and pattern recognition*, pages 14862–14870, 2021. 1, 2

[30] Lukas Hoyer, Dengxin Dai, Haoran Wang, and Luc Van Gool. Mic: Masked image consistency for context-enhanced domain adaptation. In *Proceedings of the IEEE/CVF conference on computer vision and pattern recognition*, pages 11721–11732, 2023. 6

[31] Cheng-Chun Hsu, Yi-Hsuan Tsai, Yen-Yu Lin, and Ming-Hsuan Yang. Every pixel matters: Center-aware feature alignment for domain adaptive object detector. In *Computer Vision–ECCV 2020: 16th European Conference, Glasgow, UK, August 23–28, 2020, Proceedings, Part IX 16*, pages 733–748. Springer, 2020. 1

[32] Xiaowei Hu, Chi-Wing Fu, Lei Zhu, and Pheng-Ann Heng. Depth-attentional features for single-image rain removal. In *Proceedings of the IEEE/CVF Conference on Computer Vision and Pattern Recognition (CVPR)*, 2019. 5

[33] Jiaxing Huang, Dayan Guan, Aoran Xiao, and Shijian Lu. Fsdr: Frequency space domain randomization for domain generalization. In *Proceedings of the IEEE/CVF conference on computer vision and pattern recognition*, pages 6891–6902, 2021. 6

[34] Lei Huang, Yi Zhou, Fan Zhu, Li Liu, and Ling Shao. Iterative normalization: Beyond standardization towards efficient whitening. In *Proceedings of the IEEE/CVF conference on computer vision and pattern recognition*, pages 4874–4883, 2019. 3

[35] Naoto Inoue, Ryosuke Furuta, Toshihiko Yamasaki, and Kiyoharu Aizawa. Cross-domain weakly-supervised object detection through progressive domain adaptation. In *Proceedings of the IEEE conference on computer vision and pattern recognition*, pages 5001–5009, 2018. 5

[36] Yuxiang Ji, Boyong He, Chenyuan Qu, Zhuoyue Tan, Chuan Qin, and Liaoni Wu. Diffusion features to bridge domain gap for semantic segmentation. *arXiv preprint arXiv:2406.00777*, 2024. 3

[37] Junguang Jiang, Baixu Chen, Jianmin Wang, and Ming-sheng Long. Decoupled adaptation for cross-domain object detection. In *International Conference on Learning Representations*, 2021. 2, 3

[38] Matthew Johnson-Roberson, Charles Barto, Rounak Mehta, Sharath Nittur Sridhar, Karl Rosaen, and Ram Vasudevan. Driving in the matrix: Can virtual worlds replace human-generated annotations for real world tasks? In *2017 IEEE International Conference on Robotics and Automation (ICRA)*. IEEE, 2017. 5

[39] Seunghyeon Kim, Jaehoon Choi, Taekyung Kim, and Changick Kim. Self-training and adversarial background regularization for unsupervised domain adaptive one-stage object detection. In *Proceedings of the IEEE/CVF International Conference on Computer Vision*, pages 6092–6101, 2019. 2

[40] Fabian Kuppers, Jan Kronenberger, Amirhossein Shantia, and Anselm Haselhoff. Multivariate confidence calibration for object detection. In *Proceedings of the IEEE/CVF conference on computer vision and pattern recognition workshops*, pages 326–327, 2020. 7

[41] Wooju Lee, Dasol Hong, Hyungtae Lim, and Hyun Myung. Object-aware domain generalization for object detection. In *Proceedings of the AAAI Conference on Artificial Intelligence*, pages 2947–2955, 2024. 1, 2, 5, 6, 8, 3

[42] Da Li, Jianshu Zhang, Yongxin Yang, Cong Liu, Yi-Zhe Song, and Timothy M Hospedales. Episodic training for domain generalization. In *Proceedings of the IEEE/CVF International Conference on Computer Vision*, pages 1446–1455, 2019. 1

[43] Haoliang Li, Sinno Jialin Pan, Shiqi Wang, and Alex C Kot. Domain generalization with adversarial feature learning. In *Proceedings of the IEEE conference on computer vision and pattern recognition*, pages 5400–5409, 2018. 1

[44] Haoliang Li, Sinno Jialin Pan, Shiqi Wang, and Alex C Kot. Domain generalization with adversarial feature learning. In *Proceedings of the IEEE conference on computer vision and pattern recognition*, pages 5400–5409, 2018. 1, 2

[45] Liunian Harold Li, Pengchuan Zhang, Haotian Zhang, Jianwei Yang, Chunyuan Li, Yiwu Zhong, Lijuan Wang, Lu Yuan, Lei Zhang, Jenq-Neng Hwang, et al. Grounded language-image pre-training. In *Proceedings of the IEEE/CVF Conference on Computer Vision and Pattern Recognition*, pages 10965–10975, 2022. 7, 8

[46] Shuai Li, Jianqiang Huang, Xian-Sheng Hua, and Lei Zhang. Category dictionary guided unsupervised domain adaptation for object detection. In *Proceedings of the AAAI conference on artificial intelligence*, pages 1949–1957, 2021. 2

[47] Shuaifeng Li, Mao Ye, Xiatian Zhu, Lihua Zhou, and Lin Xiong. Source-free object detection by learning to overlook domain style. In *Proceedings of the IEEE/CVF Conference*

on Computer Vision and Pattern Recognition, pages 8014–8023, 2022. 2

[48] Wuyang Li, Xinyu Liu, and Yixuan Yuan. Sigma: Semantic-complete graph matching for domain adaptive object detection. In *Proceedings of the IEEE/CVF Conference on Computer Vision and Pattern Recognition*, pages 5291–5300, 2022. 6

[49] Wuyang Li, Xinyu Liu, and Yixuan Yuan. Sigma++: Improved semantic-complete graph matching for domain adaptive object detection. *IEEE Transactions on Pattern Analysis and Machine Intelligence*, 2023. 6

[50] Yu-Jhe Li, Xiaoliang Dai, Chih-Yao Ma, Yen-Cheng Liu, Kan Chen, Bichen Wu, Zijian He, Kris Kitani, and Peter Vajda. Cross-domain adaptive teacher for object detection. In *Proceedings of the IEEE/CVF Conference on Computer Vision and Pattern Recognition*, pages 7581–7590, 2022. 1, 2, 5, 6, 3

[51] Tsung-Yi Lin, Priya Goyal, Ross Girshick, Kaiming He, and Piotr Dollár. Focal loss for dense object detection. In *Proceedings of the IEEE international conference on computer vision*, pages 2980–2988, 2017. 1

[52] Yabo Liu, Jinghua Wang, Chao Huang, Yaowei Wang, and Yong Xu. Cigar: Cross-modality graph reasoning for domain adaptive object detection. In *Proceedings of the IEEE/CVF Conference on Computer Vision and Pattern Recognition*, pages 23776–23786, 2023. 6, 3

[53] Yajing Liu, Shijun Zhou, Xiyao Liu, Chunhui Hao, Baojie Fan, and Jiandong Tian. Unbiased faster r-cnn for single-source domain generalized object detection. In *Proceedings of the IEEE/CVF Conference on Computer Vision and Pattern Recognition*, pages 28838–28847, 2024. 2, 6, 3

[54] Ze Liu, Yutong Lin, Yue Cao, Han Hu, Yixuan Wei, Zheng Zhang, Stephen Lin, and Baining Guo. Swin transformer: Hierarchical vision transformer using shifted windows. In *Proceedings of the IEEE/CVF international conference on computer vision*, pages 10012–10022, 2021. 7, 8

[55] Zhuang Liu, Hanzi Mao, Chao-Yuan Wu, Christoph Feichtenhofer, Trevor Darrell, and Saining Xie. A convnet for the 2020s. In *Proceedings of the IEEE/CVF conference on computer vision and pattern recognition*, pages 11976–11986, 2022. 7, 8

[56] Grace Luo, Lisa Dunlap, Dong Huk Park, Aleksander Holynski, and Trevor Darrell. Diffusion hyperfeatures: Searching through time and space for semantic correspondence. *Advances in Neural Information Processing Systems*, 36, 2024. 3, 1

[57] Leland McInnes, John Healy, Nathaniel Saul, and Lukas Großberger. Umap: Uniform manifold approximation and projection. *Journal of Open Source Software*, 3(29), 2018. 5

[58] Claudio Michaelis, Benjamin Mitzkus, Robert Geirhos, Evgenia Rusak, Oliver Bringmann, Alexander S Ecker, Matthias Bethge, and Wieland Brendel. Benchmarking robustness in object detection: Autonomous driving when winter is coming. *arXiv preprint arXiv:1907.07484*, 2019. 5, 6

[59] Xingang Pan, Ping Luo, Jianping Shi, and Xiaoou Tang. Two at once: Enhancing learning and generalization capacities via ibn-net. In *Proceedings of the european conference on computer vision (ECCV)*, pages 464–479, 2018. 3

[60] Xingang Pan, Xiaohang Zhan, Jianping Shi, Xiaoou Tang, and Ping Luo. Switchable whitening for deep representation learning. In *Proceedings of the IEEE/CVF international conference on computer vision*, pages 1863–1871, 2019. 3

[61] Alec Radford, Jong Wook Kim, Chris Hallacy, Aditya Ramesh, Gabriel Goh, Sandhini Agarwal, Girish Sastry, Amanda Askell, Pamela Mishkin, Jack Clark, et al. Learning transferable visual models from natural language super-vision. In *International conference on machine learning*, pages 8748–8763. PMLR, 2021. 2

[62] Aditya Ramesh, Mikhail Pavlov, Gabriel Goh, Scott Gray, Chelsea Voss, Alec Radford, Mark Chen, and Ilya Sutskever. Zero-shot text-to-image generation. In *International conference on machine learning*, pages 8821–8831. Pmlr, 2021. 2

[63] Zhijie Rao, Jingcai Guo, Luyao Tang, Yue Huang, Xinghao Ding, and Song Guo. Srdc: Semantic reasoning with compound domains for single-domain generalized object detection. *IEEE Transactions on Neural Networks and Learning Systems*, 2024. 6, 3

[64] Joseph Redmon and Ali Farhadi. Yolov3: An incremental improvement. *arXiv preprint arXiv:1804.02767*, 2018. 1

[65] Shaoqing Ren, Kaiming He, Ross Girshick, and Jian Sun. Faster r-cnn: Towards real-time object detection with region proposal networks. *IEEE transactions on pattern analysis and machine intelligence*, 39(6):1137–1149, 2016. 1, 4, 5, 6

[66] Robin Rombach, Andreas Blattmann, Dominik Lorenz, Patrick Esser, and Björn Ommer. High-resolution image synthesis with latent diffusion models. In *Proceedings of the IEEE/CVF conference on computer vision and pattern recognition*, pages 10684–10695, 2022. 6

[67] Robin Rombach, Andreas Blattmann, Dominik Lorenz, Patrick Esser, and Björn Ommer. High-resolution image synthesis with latent diffusion models. In *Proceedings of the IEEE/CVF conference on computer vision and pattern recognition*, pages 10684–10695, 2022. 1, 2

[68] Olaf Ronneberger, Philipp Fischer, and Thomas Brox. U-net: Convolutional networks for biomedical image segmentation. In *Medical image computing and computer-assisted intervention–MICCAI 2015: 18th international conference, Munich, Germany, October 5–9, 2015, proceedings, part III* 18, pages 234–241. Springer, 2015. 4

[69] Olga Russakovsky, Jia Deng, Hao Su, Jonathan Krause, Sanjeev Satheesh, Sean Ma, Zhiheng Huang, Andrej Karpathy, Aditya Khosla, Michael Bernstein, et al. Imagenet large scale visual recognition challenge. *International journal of computer vision*, 115:211–252, 2015. 5

[70] Chitwan Saharia, William Chan, Saurabh Saxena, Lala Li, Jay Whang, Emily L Denton, Kamyar Ghasemipour, Raphael Gontijo Lopes, Burcu Karagol Ayan, Tim Salimans, et al. Photorealistic text-to-image diffusion models with deep language understanding. *Advances in neural information processing systems*, 35:36479–36494, 2022. 2

[71] Kuniaki Saito, Yoshitaka Ushiku, Tatsuya Harada, and Kate Saenko. Strong-weak distribution alignment for adaptive object detection. In *Proceedings of the IEEE/CVF conference on computer vision and pattern recognition*, pages 6956–6965, 2019. 1, 2, 5, 6

[72] Christos Sakaridis, Dengxin Dai, and Luc Van Gool. Semantic foggy scene understanding with synthetic data. *International Journal of Computer Vision*, 126:973–992, 2018. 5

[73] Jiaming Song, Chenlin Meng, and Stefano Ermon. Denoising diffusion implicit models. *arXiv preprint arXiv:2010.02502*, 2020. 1, 2

[74] Bo Sun, Banghuai Li, Shengcai Cai, Ye Yuan, and Chi Zhang. Fsc: Few-shot object detection via contrastive proposal encoding. In *Proceedings of the IEEE/CVF conference on computer vision and pattern recognition*, pages 7352–7362, 2021. 8

[75] Luming Tang, Menglin Jia, Qianqian Wang, Cheng Perng Phoo, and Bharath Hariharan. Emergent correspondence from image diffusion. *Advances in Neural Information Processing Systems*, 36:1363–1389, 2023. 3, 1

[76] Zhi Tian, Chunhua Shen, Hao Chen, and Tong He. Fcos: A simple and strong anchor-free object detector. *IEEE Transactions on Pattern Analysis and Machine Intelligence*, 44(4):1922–1933, 2020. 1

[77] Vudit Vudit, Martin Engelberge, and Mathieu Salzmann. Clip the gap: A single domain generalization approach for object detection. In *CVPR*, pages 3219–3229, 2023. 1, 2, 6, 3

[78] Jiabao Wang, Yuming Chen, Zhaojun Zheng, Xiang Li, Ming-Ming Cheng, and Qibin Hou. Crosskd: Cross-head knowledge distillation for object detection. In *Proceedings of the IEEE/CVF Conference on Computer Vision and Pattern Recognition*, pages 16520–16530, 2024. 4, 1

[79] Shujun Wang, Lequan Yu, Caizi Li, Chi-Wing Fu, and Pheng-Ann Heng. Learning from extrinsic and intrinsic supervisions for domain generalization. In *European Conference on Computer Vision*, pages 159–176. Springer, 2020. 1

[80] Aming Wu and Cheng Deng. Single-domain generalized object detection in urban scene via cyclic-disentangled self-distillation. In *Proceedings of the IEEE/CVF Conference on computer vision and pattern recognition*, pages 847–856, 2022. 5, 6, 3

[81] Aming Wu, Yahong Han, Linchao Zhu, and Yi Yang. Instance-invariant domain adaptive object detection via progressive disentanglement. *IEEE Transactions on Pattern Analysis and Machine Intelligence*, 44(8):4178–4193, 2021. 2

[82] Fan Wu, Jinling Gao, Lanqing Hong, Xinbing Wang, Chenghu Zhou, and Nanyang Ye. G-nas: Generalizable neural architecture search for single domain generalization object detection. In *Proceedings of the AAAI Conference on Artificial Intelligence*, pages 5958–5966, 2024. 2, 6, 3

[83] Chang-Dong Xu, Xing-Ran Zhao, Xin Jin, and Xiu-Shen Wei. Exploring categorical regularization for domain adaptive object detection. In *Proceedings of the IEEE/CVF Conference on Computer Vision and Pattern Recognition*, pages 11724–11733, 2020. 1, 2

[84] Jiarui Xu, Sifei Liu, Arash Vahdat, Wonmin Byeon, Xiaolong Wang, and Shalini De Mello. Open-vocabulary panoptic segmentation with text-to-image diffusion models. In *Proceedings of the IEEE/CVF Conference on Computer Vision and Pattern Recognition*, pages 2955–2966, 2023. 3

[85] Mingjun Xu, Lingyun Qin, Weijie Chen, Shiliang Pu, and Lei Zhang. Multi-view adversarial discriminator: Mine the non-causal factors for object detection in unseen domains. In *Proceedings of the IEEE/CVF Conference on computer vision and pattern recognition*, pages 8103–8112, 2023. 6

[86] Qinwei Xu, Ruipeng Zhang, Ya Zhang, Yanfeng Wang, and Qi Tian. A fourier-based framework for domain generalization. In *Proceedings of the IEEE/CVF conference on computer vision and pattern recognition*, pages 14383–14392, 2021. 6

[87] Yanchao Yang and Stefano Soatto. Fda: Fourier domain adaptation for semantic segmentation. In *Proceedings of the IEEE/CVF conference on computer vision and pattern recognition*, pages 4085–4095, 2020. 6

[88] Jayeon Yoo, Inseop Chung, and Nojun Kwak. Unsupervised domain adaptation for one-stage object detector using offsets to bounding box. In *European Conference on Computer Vision*, pages 691–708. Springer, 2022. 6

[89] Fisher Yu, Haofeng Chen, Xin Wang, Wenqi Xian, Yingying Chen, Fangchen Liu, Vashisht Madhavan, and Trevor Darrell. Bdd100k: A diverse driving dataset for heterogeneous multitask learning. In *Proceedings of the IEEE/CVF conference on computer vision and pattern recognition*, pages 2636–2645, 2020. 5

[90] Jinze Yu, Jiaming Liu, Xiaobao Wei, Haoyi Zhou, Yohei Nakata, Denis Gudovskiy, Tomoyuki Okuno, Jianxin Li, Kurt Keutzer, and Shanghang Zhang. Mttrans: Cross-domain object detection with mean teacher transformer. In *European Conference on Computer Vision*, pages 629–645. Springer, 2022. 6

[91] Liang Zhao and Limin Wang. Task-specific inconsistency alignment for domain adaptive object detection. In *Proceedings of the IEEE/CVF Conference on Computer Vision and Pattern Recognition*, pages 14217–14226, 2022. 3

[92] Yuyang Zhao, Zhun Zhong, Na Zhao, Nicu Sebe, and Gim Hee Lee. Style-hallucinated dual consistency learning for domain generalized semantic segmentation. In *European conference on computer vision*, pages 535–552. Springer, 2022. 6

[93] Zhen Zhao, Yuhong Guo, Haifeng Shen, and Jieping Ye. Adaptive object detection with dual multi-label prediction. In *Computer Vision–ECCV 2020: 16th European Conference, Glasgow, UK, August 23–28, 2020, Proceedings, Part XXVIII 16*, pages 54–69. Springer, 2020. 2

[94] Kaiyang Zhou, Yongxin Yang, Yu Qiao, and Tao Xiang. Domain generalization with mixstyle. *arXiv preprint arXiv:2104.02008*, 2021. 1, 2

[95] Kaiyang Zhou, Ziwei Liu, Yu Qiao, Tao Xiang, and Chen Change Loy. Domain generalization: A survey. *IEEE Transactions on Pattern Analysis and Machine Intelligence*, 45(4):4396–4415, 2022. 1

- [96] Wenzhang Zhou, Dawei Du, Libo Zhang, Tiejian Luo, and Yanjun Wu. Multi-granularity alignment domain adaptation for object detection. In *Proceedings of the IEEE/CVF Conference on Computer Vision and Pattern Recognition*, pages 9581–9590, 2022. [2](#), [6](#)
- [97] Wenzhang Zhou, Heng Fan, Tiejian Luo, and Libo Zhang. Unsupervised domain adaptive detection with network stability analysis. In *Proceedings of the IEEE/CVF International Conference on Computer Vision*, pages 6986–6995, 2023. [6](#)
- [98] Jun-Yan Zhu, Taesung Park, Phillip Isola, and Alexei A Efros. Unpaired image-to-image translation using cycle-consistent adversarial networks. In *Proceedings of the IEEE international conference on computer vision*, pages 2223–2232, 2017. [1](#)
- [99] Wei Zhu, Le Lu, Jing Xiao, Mei Han, Jiebo Luo, and Adam P Harrison. Localized adversarial domain generalization. In *Proceedings of the IEEE/CVF Conference on Computer Vision and Pattern Recognition*, pages 7108–7118, 2022. [1](#), [2](#)
- [100] Xizhou Zhu, Weijie Su, Lewei Lu, Bin Li, Xiaogang Wang, and Jifeng Dai. Deformable detr: Deformable transformers for end-to-end object detection. In *International Conference on Learning Representations*, 2021. [1](#)

A. Overview of Supplementary Material

This supplementary material provides additional experimental results, implementation details, and analysis to support our main paper. The contents are organized as follows:

- **Additional Description for Methods:** Detailed motivations and derivations for our proposed approach, including diffusion features for DG detection, two-level guidance framework, feature alignment, and object-level alignment mechanism (in Sec. B).
- **Class-wise Results Analysis:** Detailed per-category performance analysis on Real to Artistic and Diverse Weather benchmarks (in Sec. C).
- **Additional Results of Different SD Versions:** Comprehensive comparison and analysis of different Stable Diffusion versions (SD-1.5, SD-2.1, SD-3-M) across various benchmarks (in Sec. D).
- **Additional Analysis for Results:** In-depth analysis of domain distribution differences and confusion matrix patterns to validate our method’s effectiveness (in Sec. E).
- **Visualization of Detection Results:** Qualitative results demonstrating our method’s superior performance across different domain generalization scenarios (in Sec. F).

List of Tables:

- **Class-wise Results Tables:**

- Results on Comic dataset (Tab. 12)
- Results on Watercolor dataset (Tab. 13)
- Results on Diverse Weather benchmark (Tab. 14)
- Results on Clipart dataset (Tab. 15)

- **Model Comparison Tables:**

- Comparison of different SD versions (Tab. 16)

List of Figures:

- **Analysis Visualizations:**

- Domain distribution visualization (Fig. 7)
- Confusion matrices on FoggyCityscapes (Fig. 8)
- Confusion matrices on Clipart (Fig. 9)

- **Detection Results:**

- Qualitative results on BDD100K (Fig. 10)
- Qualitative results on FoggyCityscapes (Fig. 11)
- Qualitative results on Cityscapes (Car) (Fig. 12)
- Qualitative results on Clipart (Fig. 13)
- Qualitative results on Diverse Weather Benchmark (Fig. 14)
- Qualitative results on Corruption Benchmark (Fig. 15)

B. Additional Description for Methods

B.1. Motivations

Diffusion features for DG detection. Domain generalization for object detection requires learning domain-invariant representations without accessing target domain data, which remains challenging due to complex real-world variations. While existing detectors struggle under domain shifts [95],

diffusion models have demonstrated unique advantages in handling diverse variations through their progressive denoising process. These models naturally distinguish intrinsic semantic structures from domain-specific variations [56, 75], building robustness against various perturbations. We leverage these properties for domain-generalized detection: the denoising mechanism filters out domain-specific variations while preserving essential object characteristics [24], and the multi-scale features provide robust semantic representations that generalize across domains.

Two-level guidance from frozen diffusion detector. While directly using diffusion features provides strong generalization capability, it incurs substantial computational overhead. This motivates us to transfer the generalization ability from a frozen diffusion detector to lightweight detectors. We propose a two-level guidance framework to capture both semantic understanding and detection knowledge. At the feature level, we align global feature distributions between diffusion and conventional detectors to learn domain-invariant representations. At the object level, we facilitate task-specific knowledge transfer through shared detection heads following [78], enabling precise localization and classification learning from the diffusion teacher.

Feature alignment for heterogeneous detectors. Direct feature alignment with MSE leads to suboptimal results due to different magnitude distributions and feature dominance issues [4]. We leverage Pearson Correlation Coefficient (PCC) for feature alignment, which captures relational patterns while being invariant to magnitude differences. By normalizing features before alignment, PCC effectively handles discrepancies between diffusion and conventional detectors, enabling stable knowledge transfer between heterogeneous detector pairs.

Object-level alignment for task-specific knowledge transfer. While feature-level alignment helps learn domain-invariant representations, detection-specific knowledge transfer remains challenging due to architectural differences. We propose an object-level alignment scheme that shares detection heads between student and teacher [78], providing task-oriented supervision through classification and regression branches. This complementary guidance enables effective knowledge transfer from the diffusion teacher to conventional detectors.

C. Classwise Results

Results on Real to Artistic: As shown in Tab. 15, 12, and 13, our diffusion detector demonstrates remarkable generalization capability on artistic-style datasets, surpassing both DG and DA methods significantly. On Clipart, our diffusion detector achieves 58.3% mAP, leading to substantial improvements of 9.0% and 19.4% over the previous best DA method AT [50] and DG method DivAlign [16], respectively. On Comic dataset, our method reaches 51.9%

mAP, exhibiting clear advantages compared to the best DA approach D-ADAPT [37] at 40.5% and DG method DivAlign [16] at 33.2%. For Watercolor, we achieve 68.4% mAP, which significantly surpasses the previous best results of 59.9% from AT [50] and 57.4% from DivAlign [16].

However, the diffusion-guided detector shows limited success in bridging extreme domain gaps. On Clipart, Comic, and Watercolor, the diffusion-guided detector (40.8%, 29.7%, and 54.2% respectively) underperforms compared to both recent DG methods (DivAlign: 38.9%, 33.2%, and 57.4%) and DA approaches (AT and D-ADAPT: 49.3%, 40.5%, and 59.9%). While the improvements over baseline remain notable (+13.6%, +11.6%, and +12.7% respectively), the performance gap suggests that transferring the strong generalization capability from diffusion models to conventional detectors remains challenging when facing significant stylistic variations, likely due to the extreme domain shifts in artistic styles that make feature alignment particularly difficult.

Results on Diverse Weather Benchmark: As shown in Tab. 14, our method demonstrates strong robustness across various weather and lighting conditions. For Daytime-Foggy scenarios, our diffusion guided detector achieves 44.7% mAP, exceeding the previous best result from UFR [53] by 5.1%. In Night-Sunny conditions, we obtain 49.1% mAP, surpassing G-NAS [82] which achieves 45.0%. The improvement becomes more pronounced in challenging Night-Rainy scenarios, where our diffusion detector reaches 27.8% mAP, considerably outperforming the previous best of 24.1% from DivAlign [16]. Under Dusk-Rainy conditions, we achieve 42.5% mAP, marking a clear advancement over DivAlign [16] at 38.1%. Most notably, the diffusion-guided detector demonstrates consistent improvements over the baseline across all four scenarios, with remarkable margins of +15.9%, +17.7%, +9.3%, and +13.3%. These comprehensive results not only validate the effectiveness of our knowledge transfer framework in handling natural environmental variations but also confirm our approach’s strong capability in enhancing detection generalization across diverse real-world conditions.

Table 12. Real to Artistic DG and DA Results (%) on Comic (Classwise).

Methods	Bike	Bird	Car	Cat	Dog	Person	mAP
DG methods (without target data)							
Div. [16] (CVPR’24)	41.7	12.3	29.0	13.2	20.6	36.5	25.5
DivAlign [16] (CVPR’24)	54.1	16.9	30.1	25.0	27.4	45.9	33.2
DA methods (with unlabeled target data)							
DA-Faster [11] (CVPR’18)	31.1	10.3	15.5	12.4	19.3	39.0	21.2
SWDA [71] (CVPR’19)	36.4	21.8	29.8	15.1	23.5	49.6	29.4
STABR [39] (ICCV’19)	50.6	13.6	31.0	7.5	16.4	41.4	26.8
MCRA [93] (ECCV’20)	47.9	20.5	37.4	20.6	24.5	50.2	33.5
I3Net [8] (CVPR’21)	47.5	19.9	33.2	11.4	19.4	49.1	30.1
DBGL [7] (ICCV’21)	35.6	20.3	33.9	16.4	26.6	45.3	29.7
D-ADAPT [37] (ICLR’22)	52.4	25.4	42.3	43.7	25.7	53.5	40.5
Ours (DG settings)							
Diff. Detector (SD-1.5)	63.3	41.7	58.2	<u>31.8</u>	40.9	75.3	51.9
Diff. Detector (SD-2.1)	<u>61.1</u>	<u>35.7</u>	<u>53.6</u>	23.2	<u>35.0</u>	<u>71.2</u>	<u>46.6</u>
Diff. Guided (SD-1.5)	47.6	21.0	35.3	9.1	21.6	43.5	29.7 <u>+11.6</u>
Diff. Guided (SD-2.1)	46.4	13.2	24.2	7.5	12.3	35.8	24.9 <u>+6.8</u>

Table 13. Real to Artistic DG and DA Results (%) on Watercolor (Classwise).

Methods	Bike	Bird	Car	Cat	Dog	Person	mAP
DG methods (without target data)							
Div. [16] (CVPR’24)	87.1	51.7	53.6	35.1	23.6	63.6	52.5
DivAlign [16] (CVPR’24)	90.4	51.8	51.9	43.9	35.9	70.2	57.4
DA methods (with unlabeled target data)							
SWDA [71] (CVPR’19)	82.3	55.9	46.5	32.7	35.5	66.7	53.3
MCRA [93] (ECCV’20)	87.9	52.1	51.8	41.6	33.8	68.8	56.0
UMT [17] (CVPR’21)	88.2	55.3	51.7	39.8	43.6	69.9	58.1
IIOD [81] (TPAMI’21)	95.8	54.3	48.3	42.4	35.1	65.8	56.9
I3Net [8] (CVPR’21)	81.1	49.3	46.2	35.0	31.9	65.7	51.5
SADA [12] (ICCV’21)	82.9	54.6	52.3	40.5	37.7	68.2	56.0
CDG [46] (CVPR’19)	97.7	53.1	52.1	47.3	38.7	68.9	59.7
VDD [71] (AAAI’21)	90.0	56.6	49.2	39.5	38.8	65.3	56.6
DBGL [7] (ICCV’21)	83.1	49.3	50.6	39.8	38.7	61.3	53.8
AT [50] (CVPR’22)	93.6	56.1	58.9	37.3	39.6	<u>73.8</u>	59.9
LODS [47] (CVPR’22)	95.2	53.1	46.9	37.2	<u>47.6</u>	69.3	58.2
Ours (DG settings)							
Diff. Detector (SD-1.5)	99.8	70.3	57.5	49.8	51.0	82.0	68.4
Diff. Detector (SD-2.1)	91.1	<u>65.9</u>	<u>55.7</u>	<u>47.6</u>	39.1	73.4	<u>62.1</u>
Diff. Guided (SD-1.5)	90.1	51.0	48.5	40.2	28.9	66.7	54.2 <u>+12.7</u>
Diff. Guided (SD-2.1)	<u>99.6</u>	48.4	49.1	28.4	23.4	54.2	50.6 <u>+9.1</u>

Table 14. Generalization detection Results (%) on Diverse Weather benchmark (Classwise).

Methods	Daytime-Foggy								Night-Sunny							
	Bus	Bike	Car	Motor	Person	Rider	Truck	mAP	Bus	Bike	Car	Motor	Person	Rider	Truck	mAP
IBN-Net [59] (CVPR'18)	29.9	26.1	44.5	24.4	26.2	33.5	22.4	29.6	37.8	27.3	49.6	15.1	29.2	27.1	38.9	32.1
SW [60] (ICCV'19)	30.6	26.2	44.6	25.1	30.7	34.6	23.6	30.8	38.7	29.2	49.8	16.6	31.5	28.0	40.2	33.4
IterNorm [34] (CVPR'19)	29.7	21.8	42.4	24.4	26.0	33.3	21.6	28.5	38.5	23.5	38.9	15.8	26.6	25.9	38.1	29.6
ISW [13] (CVPR'21)	29.5	26.4	49.2	27.9	30.7	34.8	24.0	31.8	38.5	28.5	49.6	15.4	31.9	27.5	41.3	33.2
CDSD [80] (CVPR'22)	32.9	28.0	48.8	29.8	32.5	38.2	24.1	33.5	40.6	35.1	50.7	19.7	34.7	32.1	43.4	36.6
CLIPGap [77] (CVPR'23)	36.1	34.3	58.0	33.1	39.0	43.9	25.1	38.5	37.7	34.3	58.0	19.2	37.6	28.5	42.9	36.9
SRCD [63] (TNNLS'24)	36.4	30.1	52.4	31.3	33.4	40.1	27.7	35.9	43.1	32.5	52.3	20.1	34.8	31.5	42.9	36.7
G-NAS [82] (AAAI'24)	32.4	31.2	57.7	31.9	38.6	38.5	24.5	36.4	46.9	40.5	67.5	26.5	50.7	35.4	47.8	45.0
OA-DG [41] (AAAI'24)	-	-	-	-	-	-	-	38.3	-	-	-	-	-	-	-	38.0
DivAlign [16] (CVPR'24)	-	-	-	-	-	-	-	37.2	-	-	-	-	-	-	-	42.5
UFR [53] (CVPR'24)	36.9	35.8	61.7	33.7	39.5	42.2	27.5	39.6	43.6	38.1	66.1	14.7	49.1	26.4	47.5	40.8
Diff. Detector (SD-1.5)	37.5	32.4	67.9	35.6	48.3	44.6	37.1	43.3	49.6	42.1	70.5	21.4	54.5	38.2	52.6	47.0
Diff. Detector (SD-2.1)	36.4	36.7	68.8	36.6	51.5	49.1	32.9	44.6	48.2	39.6	69.2	22.8	55.4	37.7	51.6	46.4
Diff. Guided (SD-1.5)	39.3	35.8	69.4	37.7	48.8	49.7	32.3	44.7+15.9	51.0	42.8	72.2	27.5	55.9	39.5	52.0	48.6+17.2
Diff. Guided (SD-2.1)	38.8	36.4	68.9	37.4	48.6	49.6	33.4	44.7+15.9	51.3	43.6	72.3	27.6	56.2	40.2	53.7	49.1+17.7
	Night-Rainy								Dusk-Rainy							
IBN-Net [59] (CVPR'18)	24.6	10.0	28.4	0.9	8.3	9.8	18.1	14.3	37.0	14.8	50.3	11.4	17.3	13.3	38.4	26.1
SW [60] (ICCV'19)	22.3	7.8	27.6	0.2	10.3	10.0	17.7	13.7	35.2	16.7	50.1	10.4	20.1	13.0	38.8	26.3
IterNorm [34] (CVPR'19)	21.4	6.7	22.0	0.9	9.1	10.6	17.6	12.6	32.9	14.1	38.9	11.0	15.5	11.6	35.7	22.8
ISW [13] (CVPR'21)	22.5	11.4	26.9	0.4	9.9	9.8	17.5	14.1	34.7	16.0	50.0	11.1	17.8	12.6	38.8	25.9
CDSD [80] (CVPR'22)	24.4	11.6	29.5	0.4	10.5	11.4	19.2	15.3	37.1	19.6	50.9	13.4	19.7	16.3	40.7	28.2
CLIPGap [77] (CVPR'23)	28.6	12.1	36.1	9.2	12.3	9.6	22.9	18.7	37.8	22.8	60.7	16.8	26.8	18.7	42.4	32.3
SRCD [63] (TNNLS'24)	26.5	<u>12.9</u>	32.4	0.8	10.2	<u>12.5</u>	24.0	17.0	39.5	21.4	50.6	11.9	20.1	17.6	40.5	28.8
G-NAS [82] (AAAI'24)	28.6	9.8	38.4	0.1	13.8	9.8	21.4	17.4	<u>44.6</u>	22.3	66.4	14.7	32.1	19.6	45.8	35.1
OA-DG [41] (AAAI'24)	-	-	-	-	-	-	-	16.8	-	-	-	-	-	-	-	33.9
DivAlign [16] (CVPR'24)	-	-	-	-	-	-	-	<u>24.1</u>	-	-	-	-	-	-	-	38.1
UFR [53] (CVPR'24)	29.9	11.8	36.1	<u>9.4</u>	13.1	10.5	23.3	19.2	37.1	21.8	67.9	16.4	27.4	17.9	43.9	33.2
Diff. Detector (SD-1.5)	42.0	15.0	53.6	6.5	26.2	13.8	37.5	27.8	49.7	27.9	74.9	18.2	45.5	24.5	56.8	42.5
Diff. Detector (SD-2.1)	30.1	11.3	46.1	10.2	<u>24.1</u>	9.2	<u>31.5</u>	23.2	<u>44.6</u>	30.6	73.5	22.1	<u>44.4</u>	20.1	<u>55.6</u>	<u>41.6</u>
Diff. Guided (SD-1.5)	<u>35.4</u>	12.7	46.2	3.2	13.8	10.7	29.7	<u>21.7+9.3</u>	43.1	23.9	73.6	13.4	33.2	<u>22.1</u>	52.3	<u>37.4+13.3</u>
Diff. Guided (SD-2.1)	34.4	7.8	43.3	2.2	14.3	7.5	30.3	<u>20.8+8.4</u>	<u>44.6</u>	22.5	73.1	15.7	31.7	19.3	52.6	<u>37.3+13.2</u>

Table 15. Real to Artistic DG and DA Results (%) on Clipart (Classwise).

Methods	aero.	bike	bird	boat	bottle	bus	car	cat	chair	cow	table	dog	horse	bike	psn.	plant.	sheep	sofa	train	tv	mAP
DG methods (without target data)																					
Div. [16] (CVPR'24)	29.3	50.9	23.4	35.3	45.3	49.8	33.4	10.6	43.3	22.3	31.6	4.5	32.9	51.9	40.2	51.1	18.2	29.6	42.3	28.5	33.7
DivAlign [16] (CVPR'24)	34.4	64.4	22.7	27.0	45.6	59.2	32.9	7.0	46.8	55.8	28.9	14.5	44.4	58.0	55.2	52.1	14.8	38.4	42.5	33.9	38.9
DA methods (with unlabeled target data)																					
AT [50] (CVPR'22)	33.8	60.9	38.6	49.4	52.4	53.9	56.7	7.5	52.8	63.5	34.0	25.0	62.2	72.1	77.2	57.7	27.2	52.0	55.7	54.1	49.3
D-ADAPT [37] (ICLR'22)	56.4	63.2	42.3	40.9	45.3	<u>77.0</u>	48.7	<u>25.4</u>	44.3	58.4	31.4	24.5	47.1	75.3	69.3	43.5	<u>27.9</u>	34.1	<u>60.7</u>	64.0	49.0
TIA [91] (CVPR'22)	42.2	<u>66.0</u>	36.9	37.3	43.7	71.8	49.7	18.2	44.9	58.9	18.2	<u>29.1</u>	40.7	<u>87.8</u>	67.4	49.7	27.4	27.8	57.1	50.6	46.3
CIGAR [52] (CVPR'23)	35.2	55.0	39.2	30.7	60.1	58.1	46.9	31.8	47.0	<u>61.0</u>	21.8	26.7	44.6	52.4	68.5	54.4	31.3	38.8	56.5	<u>63.5</u>	46.2
CMT [3] (CVPR'23)	39.8	56.3	38.7	39.7	<u>60.0</u>	35.0	56.0	7.1	60.1	60.4	35.8	28.1	67.8	84.5	80.1	55.5	20.3	32.8	42.3	38.2	47.0
<i>Ours (DG settings)</i>																					
Diff. Detector (SD-1.5)	63.7	86.1	49.8	<u>56.5</u>	52.9	50.9	67.3	19.7	74.7	34.3	57.7	41.9	<u>63.2</u>	89.4	89.6	59.8	23.5	64.9	65.9	55.2	58.3
Diff. Detector (SD-2.1)	65.5	61.7	<u>49.5</u>	58.7	59.8	34.2	63.6	20.4	<u>72.9</u>	22.2	47.1	28.5	51.2	82.3	<u>87.0</u>	61.7	20.6	<u>57.9</u>	44.6	44.2	<u>51.7</u>
Diff. Guided (SD-1.5)	19.3	57.8	28.4	37.4	57.8	81.3	46.3	3.8	57.8	27.2	28.3	19.6	42.5	50.9	57.8	<u>59.8</u>	15.6	36.0	37.7	50.5	<u>40.8+13.6</u>
Diff. Guided (SD-2.1)	25.6	40.2	26.2	25.7	44.8	72.9	34.8	3.8	46.3	14.0	26.6	7.5	27.2	57.1	48.4	56.4	6.8	25.3	24.5	39.2	<u>32.7+5.5</u>

D. Additional Results of Different Stable Diffusion Versions

Performance Comparison of Different SD Versions: Experimental results in Tab. 16 demonstrate varying performance among Stable Diffusion versions across different scenarios. SD-1.5 consistently achieves superior performance, particularly in adverse weather (50.1% for foggy, 58.2% for rainy) and artistic style transfer (58.3%, 51.9%, 68.4% for Clipart, Comic, Watercolor). While SD-2.1 maintains competitive performance and achieves 64.5% accuracy in Cityscapes car detection, it shows performance gaps of 6.6%, 5.3%, and 6.3% compared to SD-1.5 in artistic style transfer. SD-3-M shows significantly lower performance, with substantial degradation in artistic style transfer (28.7%, 24.1%, 45.0%) and diverse weather conditions (10.4% lower than SD-1.5).

Analysis of Architecture Differences: The inferior performance of SD-3-M primarily stems from its architectural differences. Unlike SD-1.5 and SD-2.1 with UNet [68] architecture that produces multi-scale hierarchical features, SD-3-M with transformer-based structure [21] outputs fixed-dimensional feature maps. This limitation affects its ability to capture fine-grained spatial information crucial for object detection, particularly impacting performance across diverse domains.

Ongoing Research: We are currently conducting extensive experiments to improve the cross-domain detection performance of SD-3-M. Our ongoing research focuses on developing effective methods to leverage the intermediate features of SD-3-M, aiming to fully utilize its strong semantic understanding capabilities while addressing the challenges in dense prediction tasks. The experimental results and detailed analysis will be reported in future work.

E. Additional Analysis for Results

E.1. Visualization of Domain Distribution Differences

Distribution Analysis: As visualized in Fig. 7, significant distribution gaps exist between source and target domains across different benchmarks. The diverse scenarios including cross-camera, adverse weather, synthetic-to-real transfer, artistic style transfer, and various weather conditions all demonstrate distinct distribution separations between source and target domains. These distribution discrepancies explain the challenges faced by conventional detectors when deploying across domains, highlighting the necessity of robust domain-generalized detection approaches.

E.2. Confusion Matrix Error Analysis

Analysis of Confusion Matrices: As shown in Fig. 8 and 9, the confusion matrices reveal that false negatives (missed

detections) are the primary factor affecting detection performance in the baseline detector. Our proposed Diff. Detector significantly reduces the probability of missed detections, as evidenced by the stronger diagonal patterns in both FoggyCityscapes and Clipart scenarios.

Through our designed feature and object alignment mechanism, the Diff. Guided Detector successfully inherits the robust detection capability from Diff. Detector, showing similar improvements in reducing missed detections. The enhanced diagonal patterns in confusion matrices validate the effectiveness of our knowledge transfer framework in improving cross-domain generalization performance.

F. Visualization of Detection Results

Visualization Results: As shown in Fig. 10, 11, 12, 13, 14, and 15, our proposed methods demonstrate superior detection performance across various challenging scenarios. Compared to the baseline detector, both Diff. Detector and Diff. Guided Detector achieve more comprehensive detection results, successfully identifying objects under different conditions such as varying scales, weather conditions, lighting variations, and artistic styles. These qualitative results consistently validate the effectiveness of our proposed diffusion-based framework in improving detection generalization across different domains.

Table 16. Testing Results of Diffusion Detector with Different Stable Diffusion versions. **SD-1.5**: Stable Diffusion v1.5, **SD-2.1**: Stable Diffusion v2.1, **SD-3-M**: Stable Diffusion v3 Medium. **Foggy**: FoggyCityscapes, **Rainy**: RainCityscapes. In Diverse Weather benchmark: **DF** (Daytime-Foggy), **DR** (Dusk-Rainy), **NR** (Night-Rainy), **NS** (Night-Sunny).

Cross Camera		Adverse Weather		Synthetic to Real		Real to Artistic			Diverse Weather benchmark			
Version	BDD100K	Foggy	Rainy	Cityscapes (car)	BDD100K (car)	Clipart	Comic	Watercolor	DF	DR	NR	NS
SD-1.5	46.6	50.1	<u>58.2</u>	<u>62.8</u>	64.4	58.3	51.9	68.4	<u>43.3</u>	42.5	27.8	47.0
SD-2.1	45.8	48.3	56.1	64.5	64.1	51.7	46.6	62.1	44.6	41.6	23.2	46.4
SD-3-M	40.4	46.1	59.1	59.7	54.2	28.7	24.1	45.0	36.0	30.5	15.9	32.8

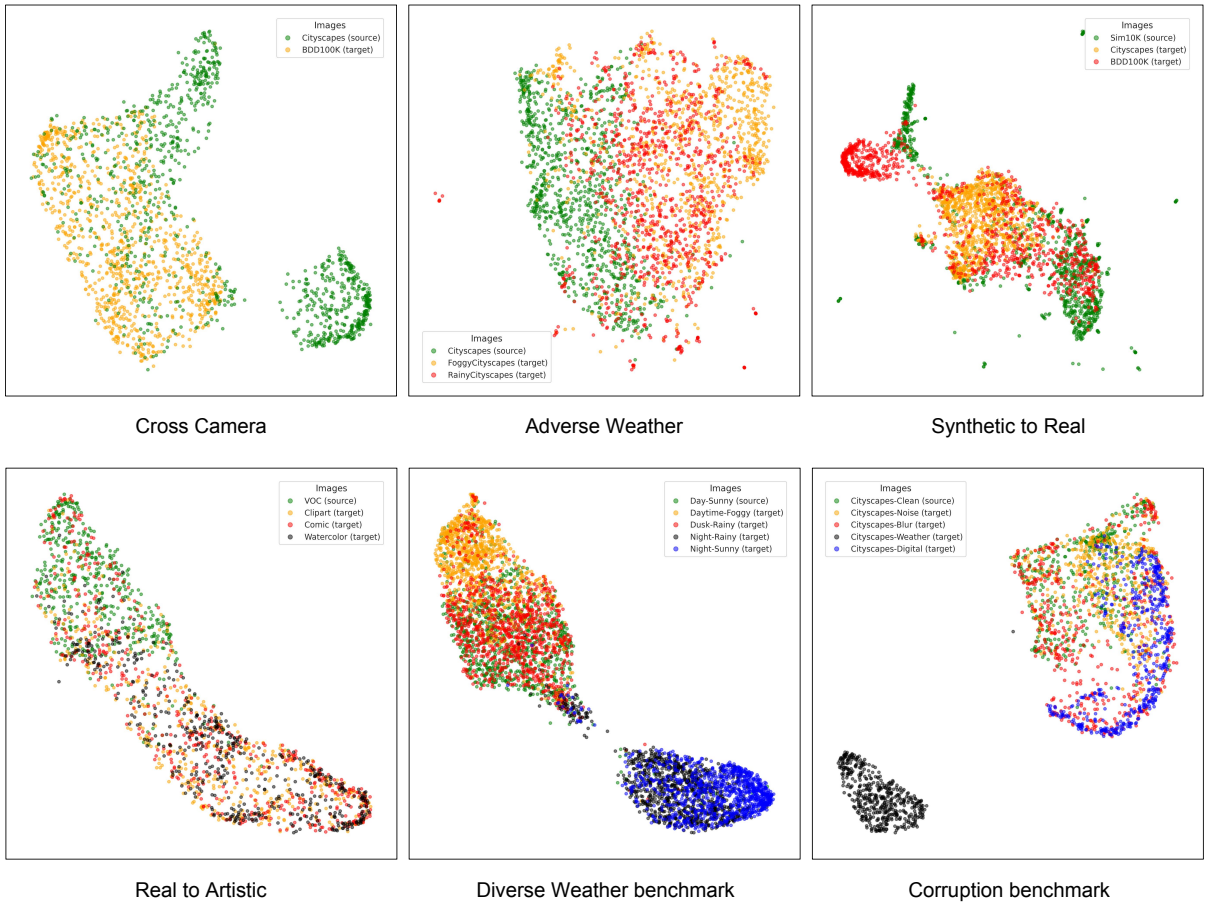


Figure 7. Image-level distribution visualization using UMAP [57] on six domain generalization benchmarks.

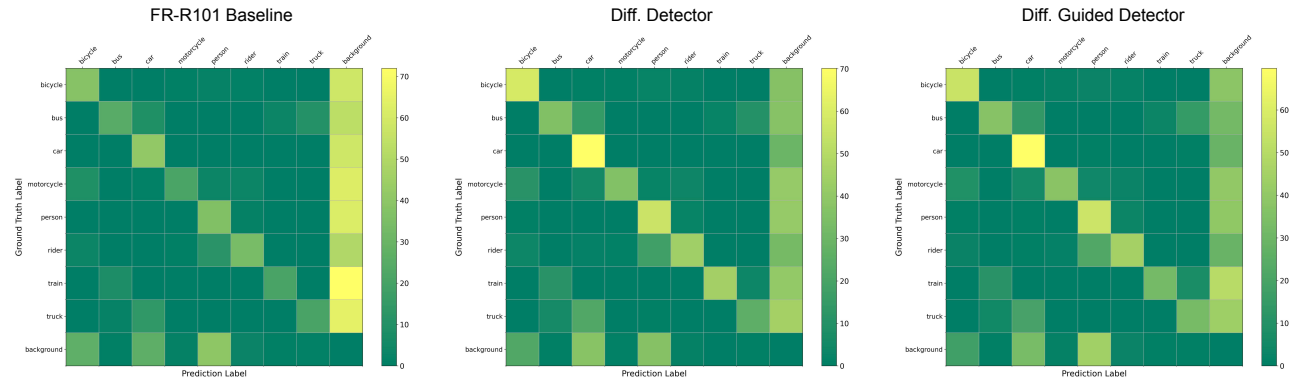


Figure 8. Confusion matrix of **Baseline** (left), **Diff. Detector** (middle), and **Diff. Guided Detector** (right) on FoggyCityscapes.

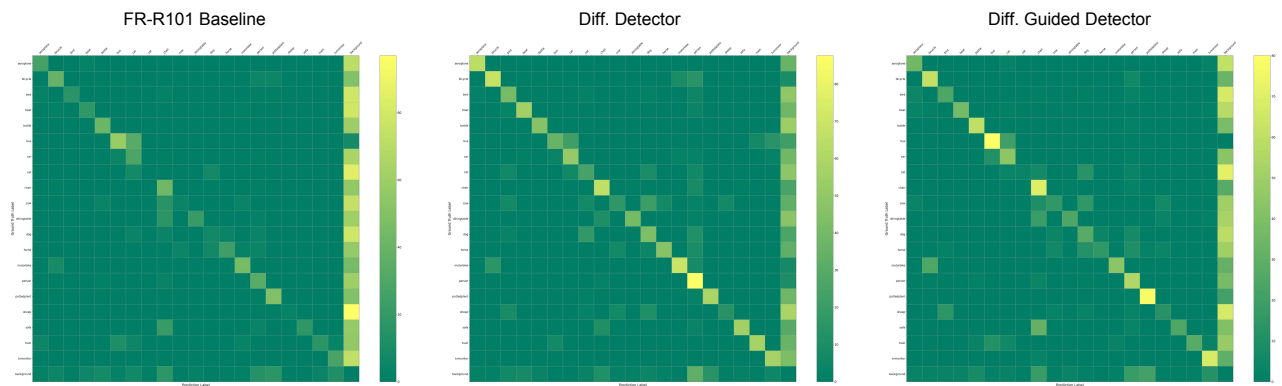


Figure 9. Confusion matrix of **Baseline** (left), **Diff. Detector** (middle), and **Diff. Guided Detector** (right) on Clipart.

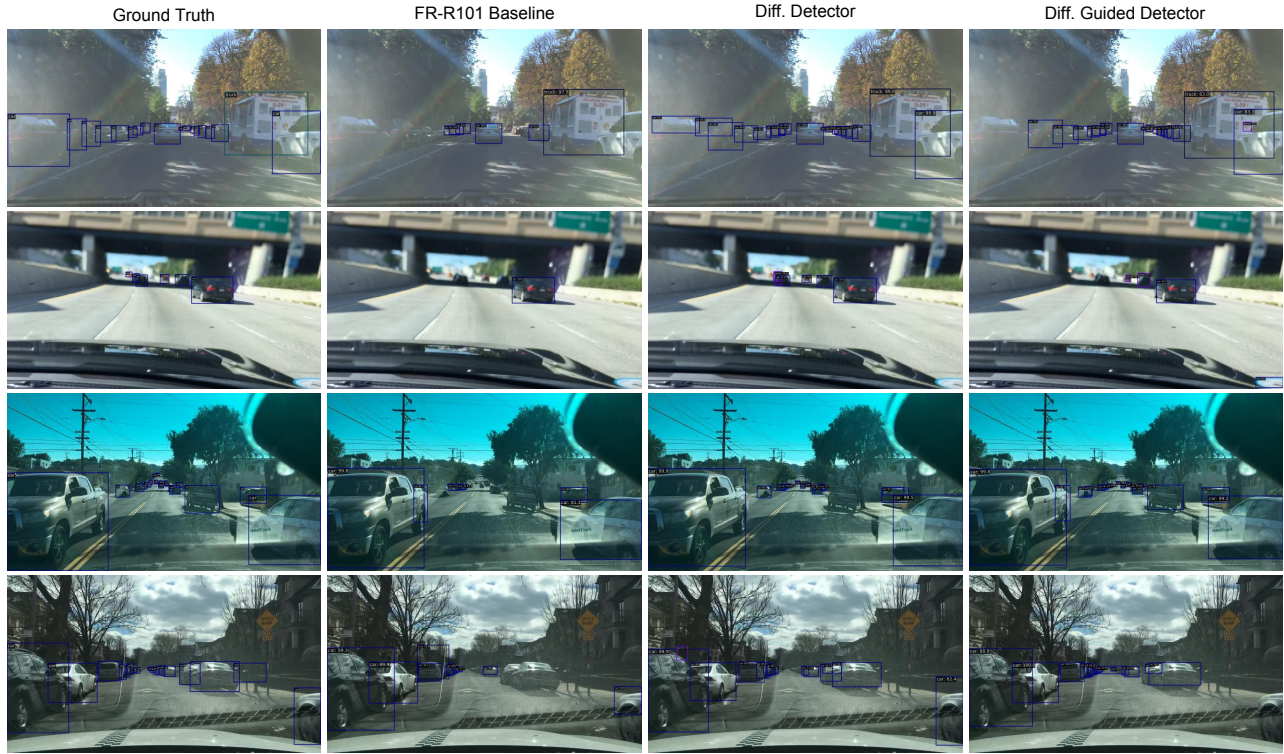


Figure 10. Qualitative prediction results on BDD100K.



Figure 11. Qualitative prediction results on FoggyCityscapes.



Figure 12. Qualitative prediction results on Cityscapes (Car).

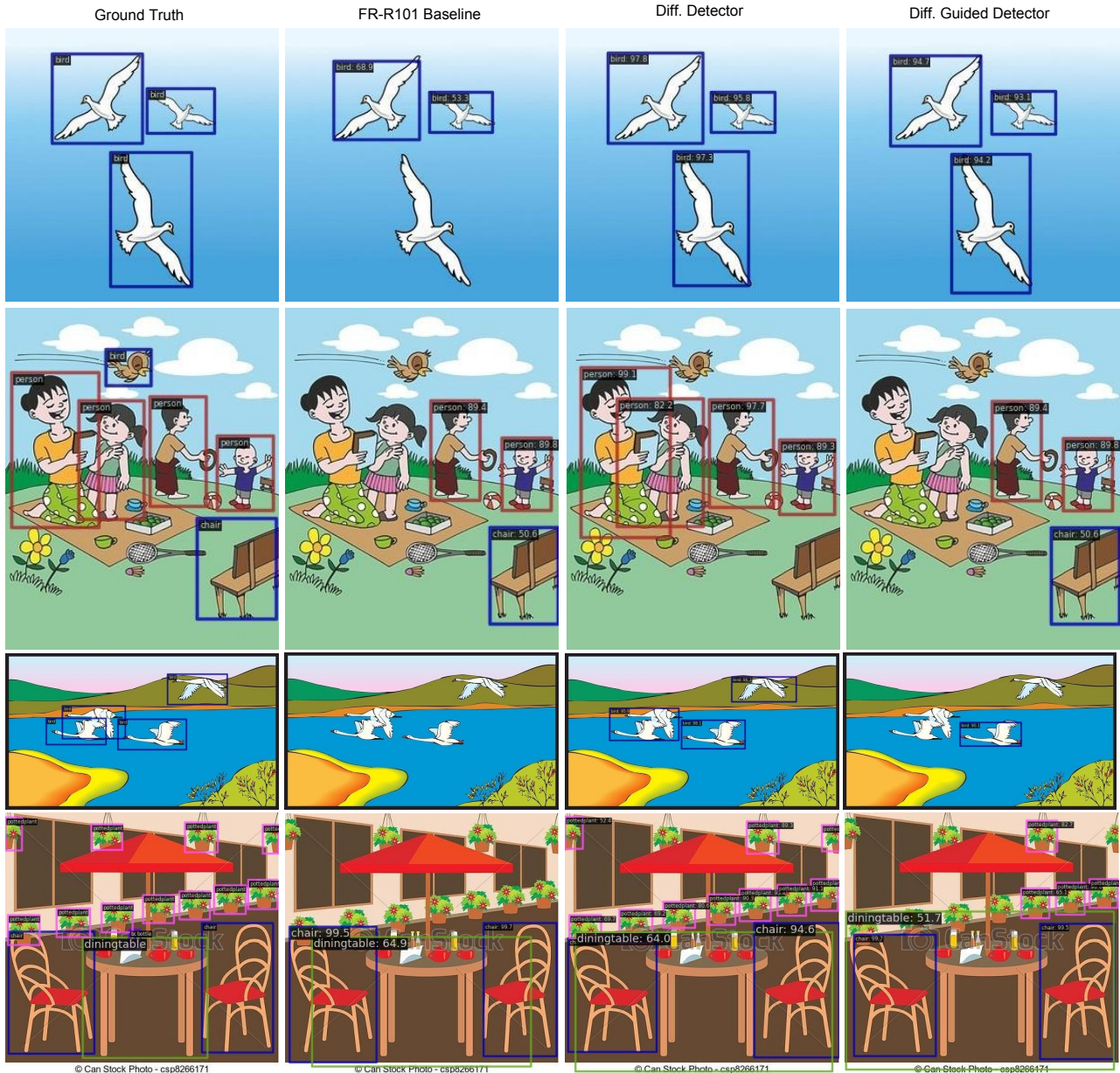


Figure 13. Qualitative prediction results on Clipart.

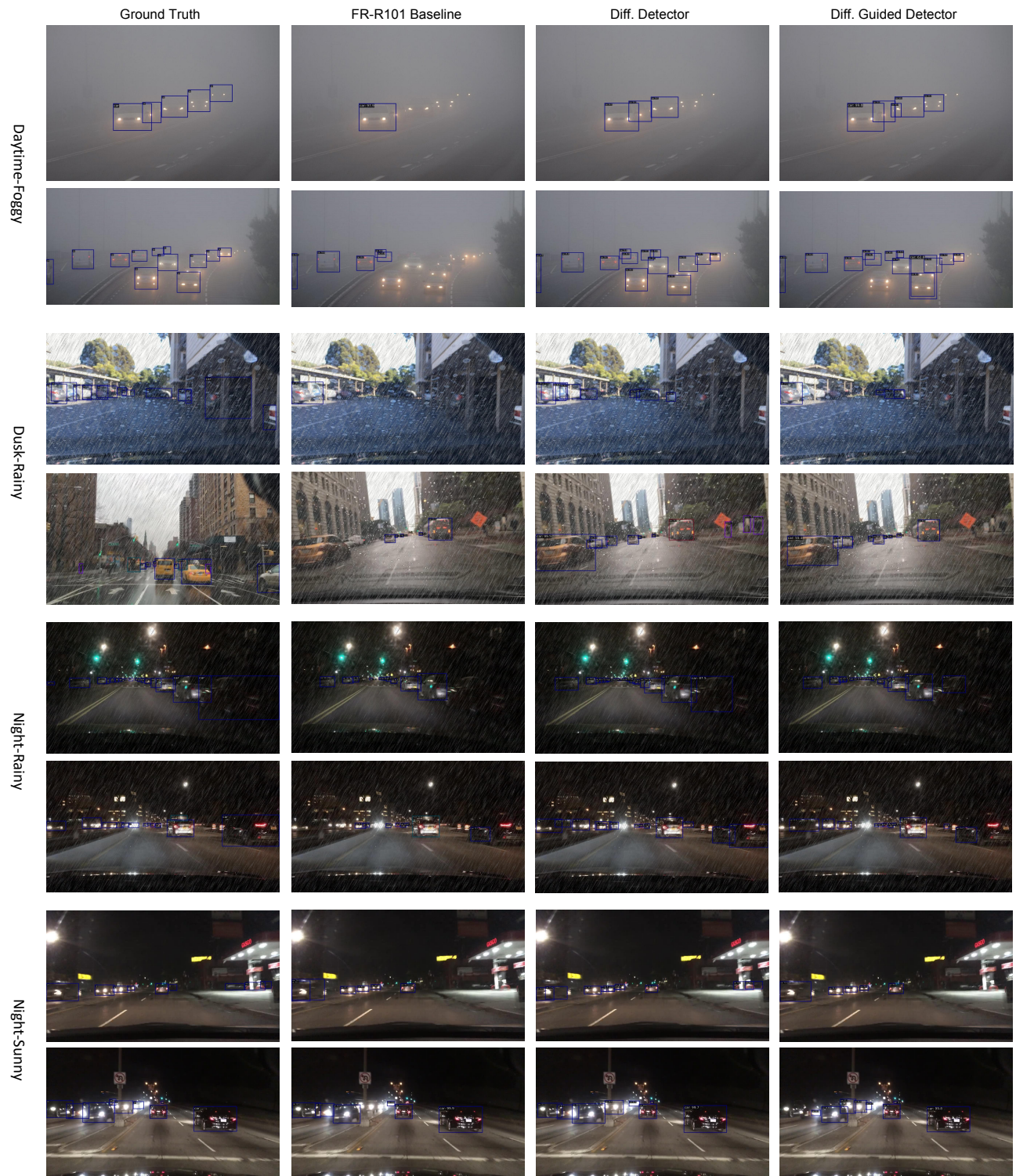


Figure 14. Qualitative prediction results on Diverse Weather Benchmark.

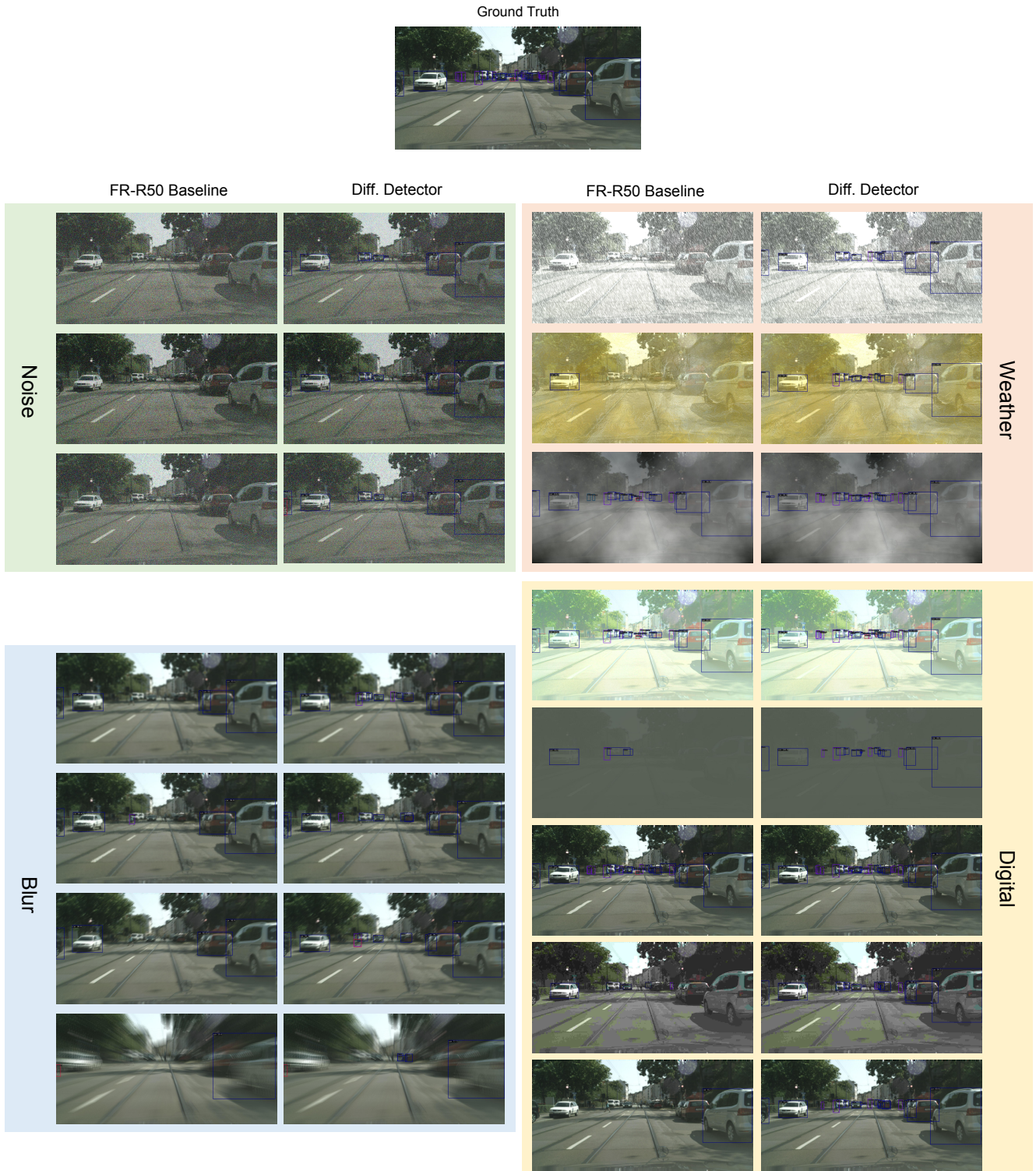


Figure 15. Qualitative prediction results on Corruption benchmark, showing detection results under 15 different corruption types (noise, blur, weather, and digital) at maximum severity level.